united nations
educational, scientific
and cultural
organization

international atomic
energy agency

the
abdus salam
international centre for theoretical physics

ICTP 40th Anniversary

SCHOOL ON SYNCHROTRON RADIATION AND APPLICATIONS
In memory of J.C. Fuggle & L. Fonda

19 April - 21 May 2004

Miramare - Trieste, Italy

1561/10

Mirrors and Gratings

D. Cocco

Mirrors and gratings

Daniele Cocco

Sincrotrone Trieste -Italy

ICTP School on Synchrotron Radiation and Application
in memory of J.C. Fuggle and L. Fonda

the abdus salam
international centre for theoretical physics

Refraction index

refractive index $\mu=1-\delta-i\beta$

$$\delta=(e^2\lambda^2/2\pi mc^2)|N+\Sigma_H N_H[\lambda/\lambda_H]^2 \ln[\lambda_H^2/\lambda^2-1]\ |$$

δ (unit decrement) related to the speed in the medium

β related to the absorption

N=electron density (10^{23}-10^{24} el./cm^3)
λ_H=adsorption edge's wavelength

λ far from $\lambda_H \Rightarrow \delta=Ne^2\lambda^2/2\pi mc^2$

$\beta=\lambda\mu_l/4\pi$ μ_l=linear absorption coefficient

Refraction index

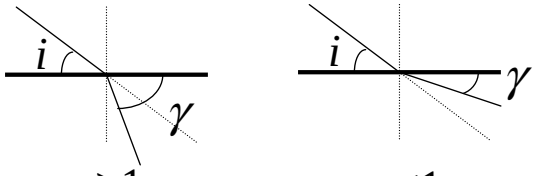

n>1 n<1

Snell's law: $\cos\gamma=\cos i/n$

$\gamma=0$ $n=\cos i_c$

i_c critical angle: total external reflection

$\sin i_c=\lambda(e^2N/\pi mc^2)^{1/2}$

$\lambda_c(\min)=3.333\cdot10^{-13}\ N^{1/2}\sin i_c$

Material	Density (g/cm^3)	N ($electron/cm^3$)	λ_{min} nm
Pentadecane (oil)	0.77	$7x10^{22}$	64.1sin*i*
Glass	2.6	$78x10^{22}$	37.9sin*i*
Aluminum oxide	3.9	$115x10^{22}$	31.2sin*i*
Gold	19.3	$466x10^{22}$	15.4sin*i*

$i=5^o$: λ_{min}glass=3.3nm=375 eV
λ_{min}gold=1.34nm=923eV

shorter wavelength needs smaller angles of incidence

Materials with higher density (i.e. higher atomic weight) have higher reflectivity

Mirror reflectivity

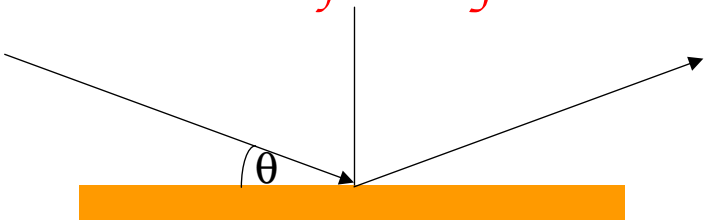

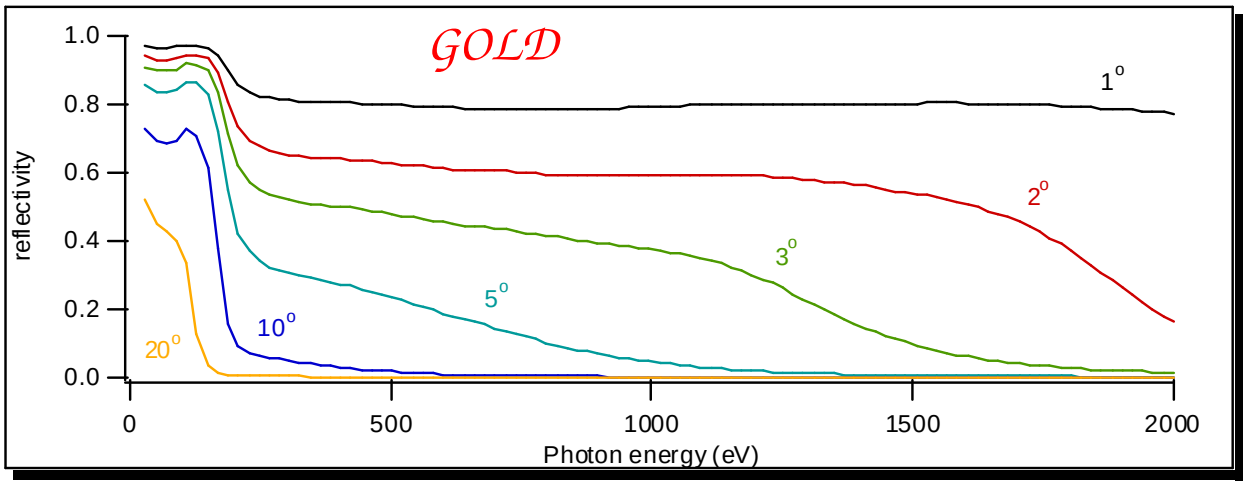

Mirror reflectivity

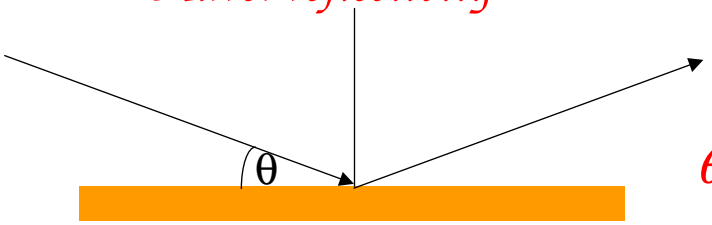

θ=2º

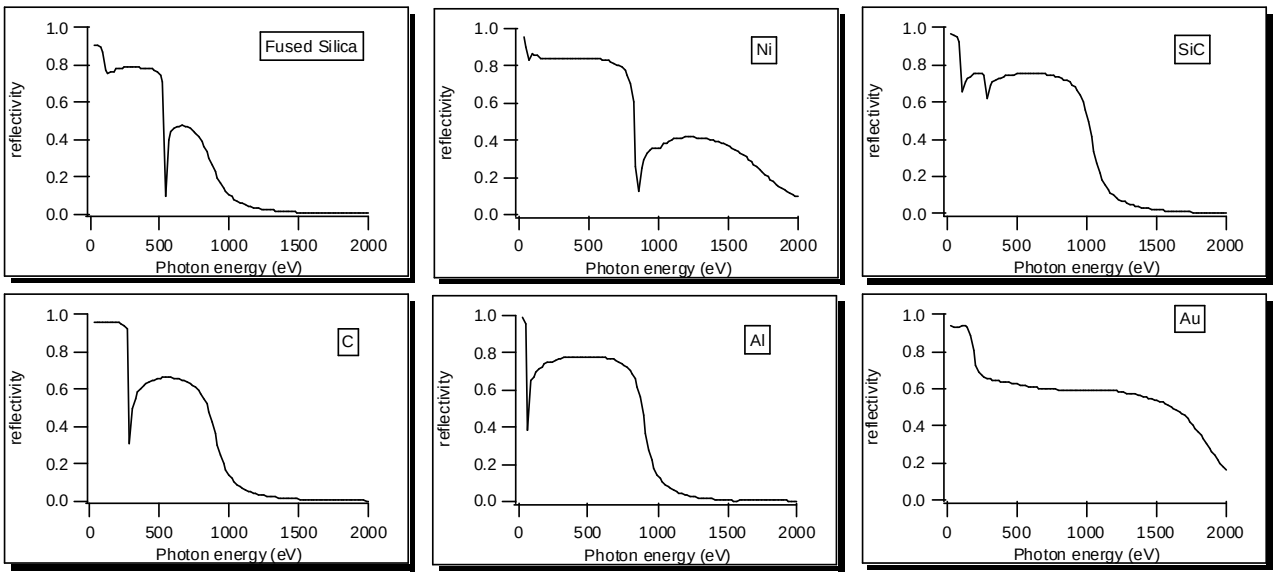

Figure errors

The error on the optics surface could be divided into two groups. The errors with period of the order of the millimetre (slope errors) and that ones with very small period (roughness)
The slope errors could be thought as imperfections that locally change the direction of the normal to the optical surface and therefore change the direction of the reflected radiation. In the following drawn δθ is the change in the normal direction and 2δθ (since the angle is doubled by the reflection) is the change in the reflected beam.

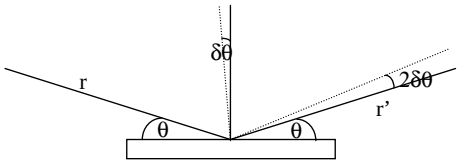

The plane drawn here is the so-called tangential plane. This is the plane designed by the normal to the optical surface and the incoming radiation. In this plane, the effect of the enlargement of the spot (s) at a distance r' from the mirror is easily estimated by:

Δs=2r'δθ tangential

In the plane perpendicular to the tangential, the so-called sagittal plane, the effect of the enlargement is reduced. As a matter of fact, an error in the direction perpendicular to the incoming rays, only introduce a deviation for the vectorial component perpendicular to the surface. Therefore the enlargement of the spot in the sagittal direction could be estimated by:

Δs=2r'δθ sin (θ) sagittal

There will be some graphs (in the nest pages) which show the spot enlargment due to the slope errors in both direction
In one r' is constant (1m) and the enlargement is plotted as a function of the slope error, in the second the slope error is fixed and the enlargement is plotted as a function of the distance from the mirror.

The second kind of error, the roughness, could be thought as a random distribution of small imperfection. In this way the final effect is a reduction of the intensity in the reflected peaks because the rays are dispersed all around the reflected beam direction and the dispersion profile follow a Gaussian distribution. The parameter of this gaussian profile depend from the ratio σ/λ where σ is the amplitude of the roughness and λ is the wavelength of the incoming radiation. Smaller is the wavelength higher is the effect of the roughness.
The intensity of the reflected radiation I is reduced with respect to the ideal reflected radiation intensity (I_0) by a factor proportional to the above mentioned ratio and precisely:

$$I = I_o e^{-\left(\frac{4\pi\sigma \sin\vartheta}{\lambda}\right)^2}$$

Figure errors

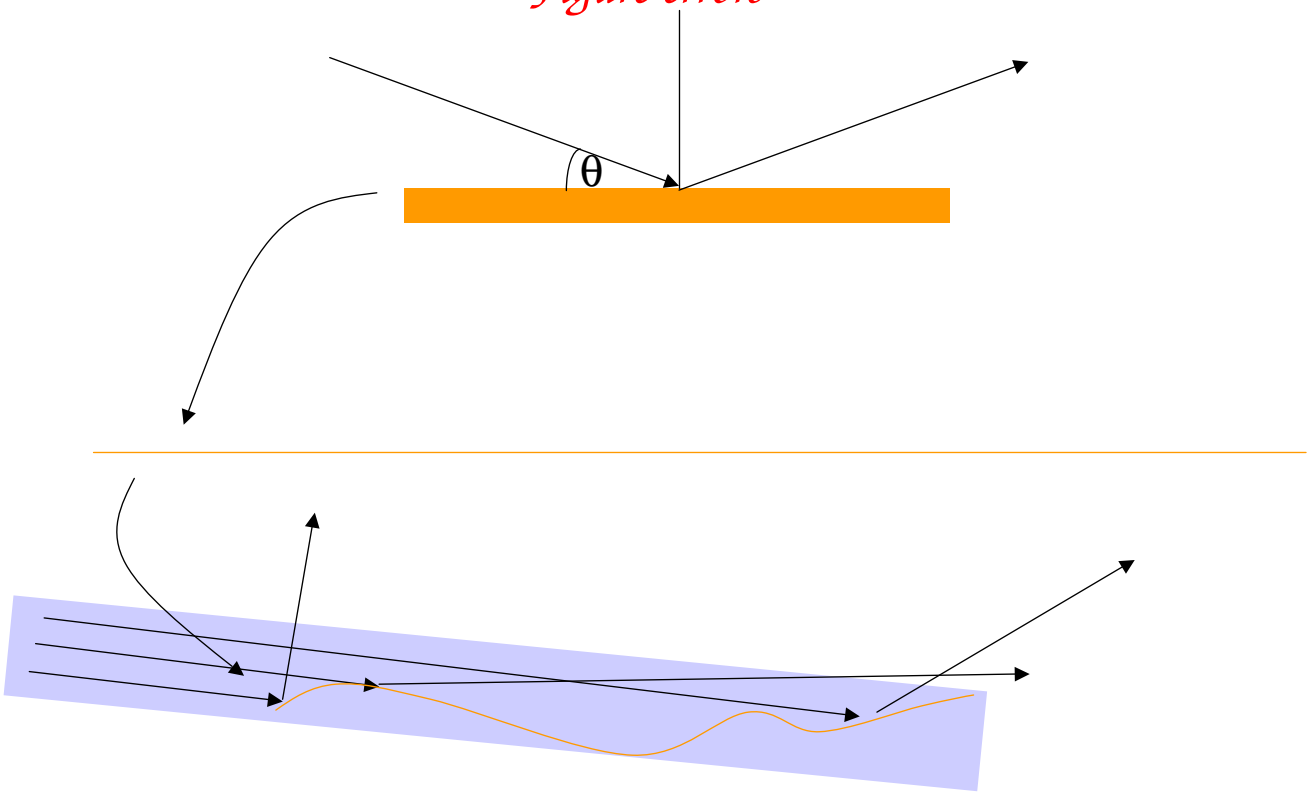

Figure errors

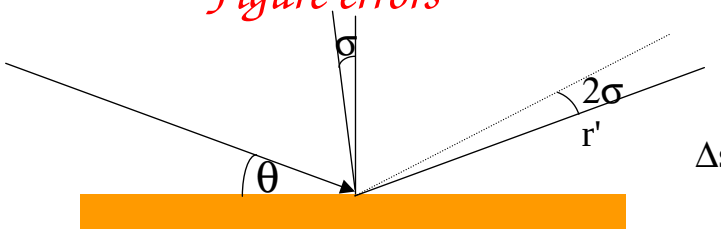

$\Delta s' = 2\, r' \sigma$

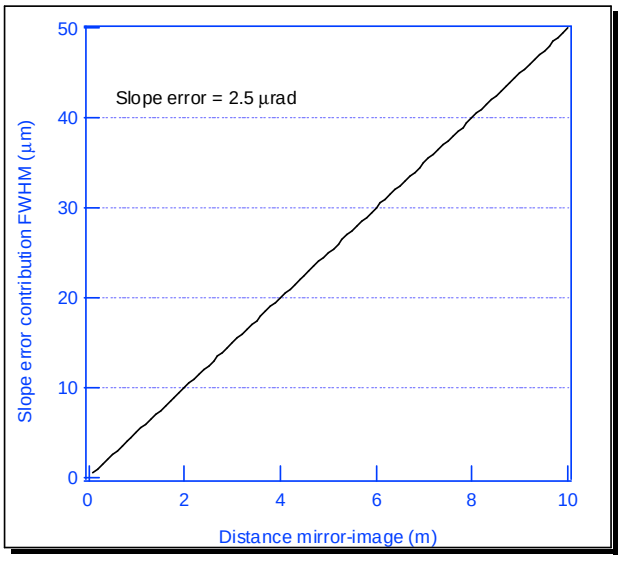

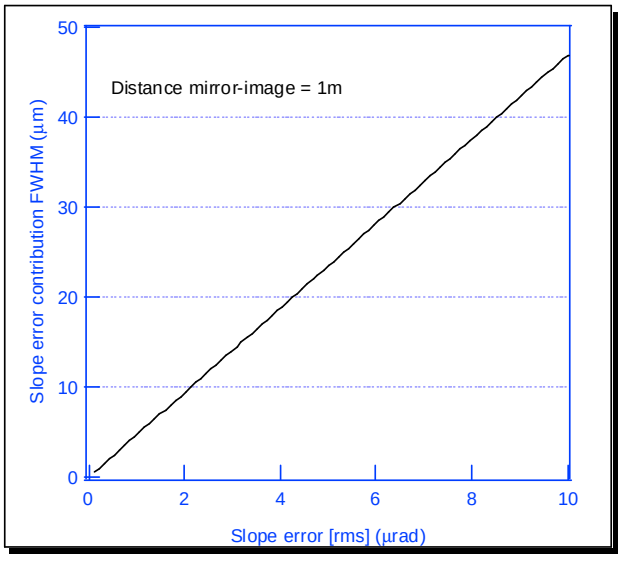

Slope errors (tangential)

Typical manufacturer capabilities (SESO, ZEISS, Winlight, Jobin Yvon)

Shape	Lenght	rms errors
Spherical/flat	Up to 500 mm	< 0.5 µrad
Spherical/flat	> 500 mm	1-2 µrad
Toroidal	Up to 500 mm	< 1 µrad
Toroidal	> 500 mm	> 1 µrad
Aspherical	Up to 500 mm	2 µrad
Aspherical	> 500 mm	3-5 µrad

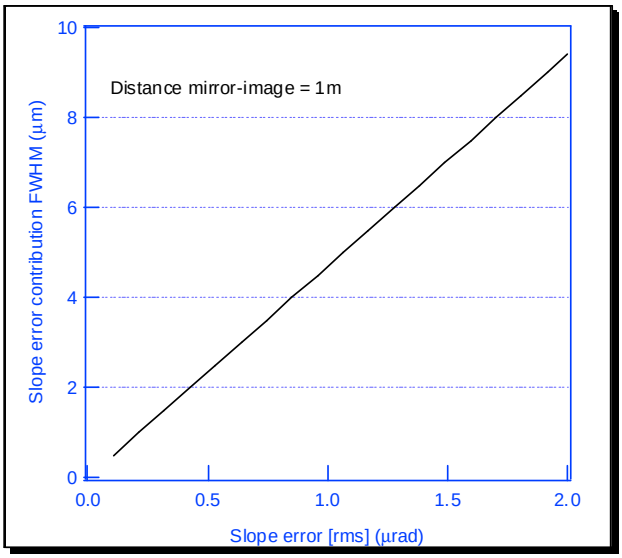

Focal property

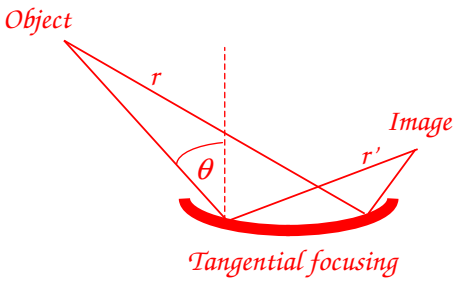

Tangential focusing

Term $\mathcal{F}_{20}$ of the optical path function

$(1/r+1/r')\cos\theta/2=1/\mathcal{R}$ spherical mirror

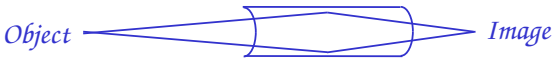

Sagital focusing

Term $\mathcal{F}_{02}$ of the optical path function

$(1/r+1/r')/(2\cos\theta)=1/\mathcal{R}$ cylindrical/toroidal mirror

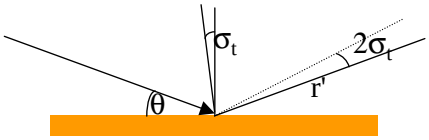

$\Delta s'_t = 2\, r' \sigma_t$

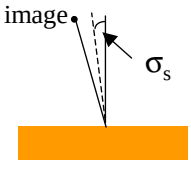

$\Delta s'_s = 2\, r' \sin\theta\, \sigma_s$

Slope error effect

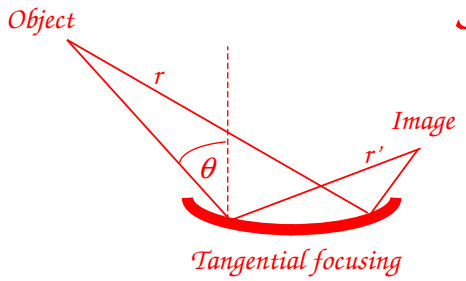

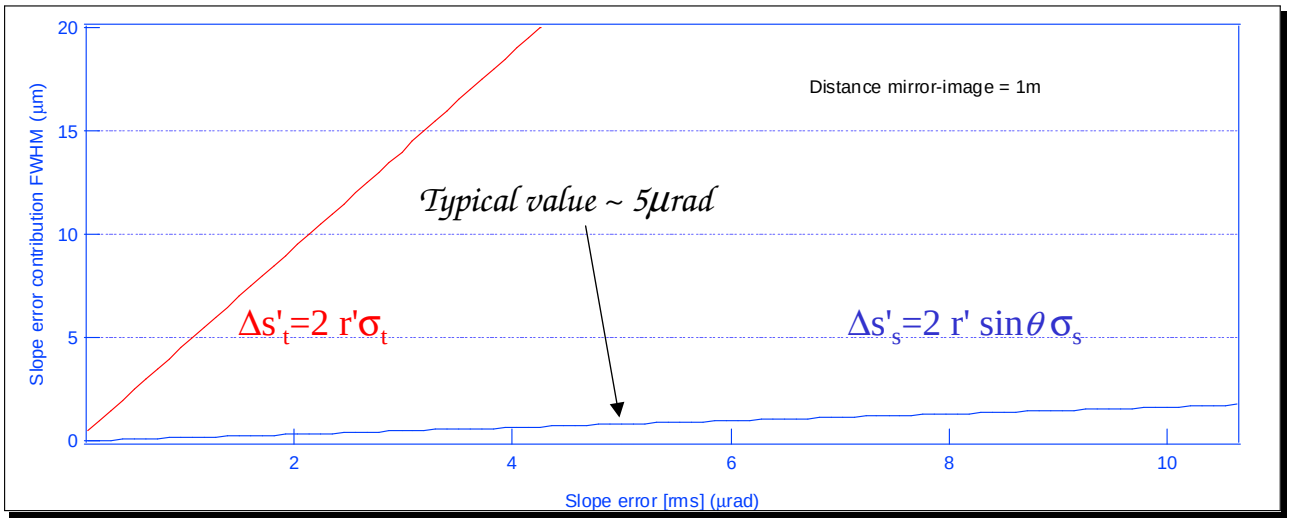

F30 effect (primary coma)

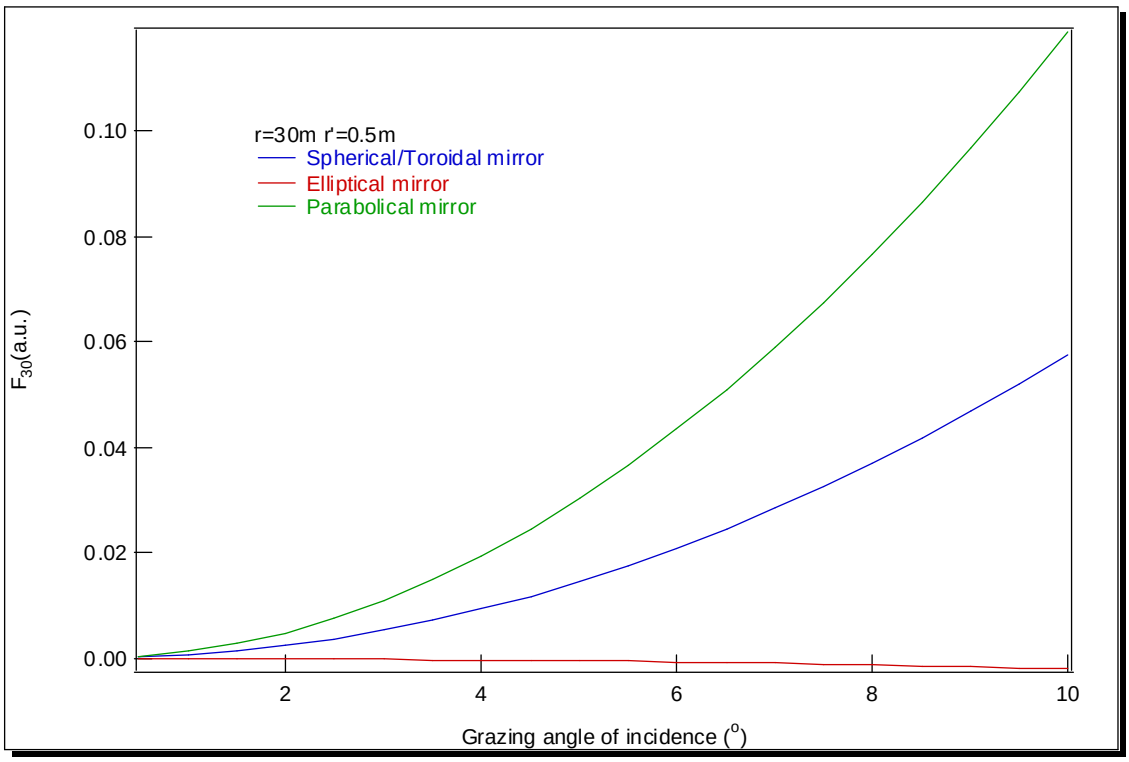

Final focus (F30-F03)

source 80 μm vertical; r=4000 mm r´ =400 mm (10:1) θ=88°

Beam divergence 100X100 μrad

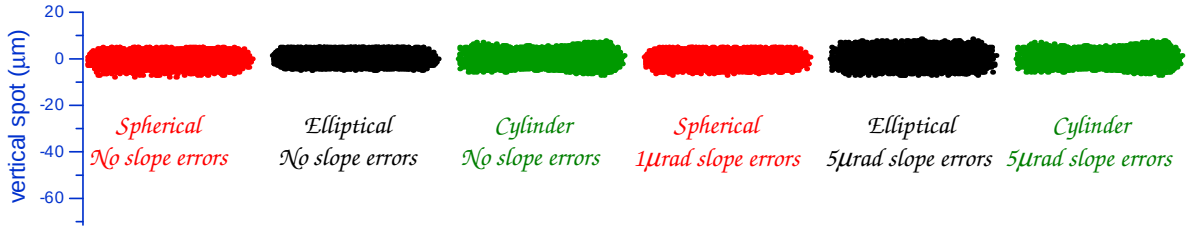

Beam divergence 500X500 μrad

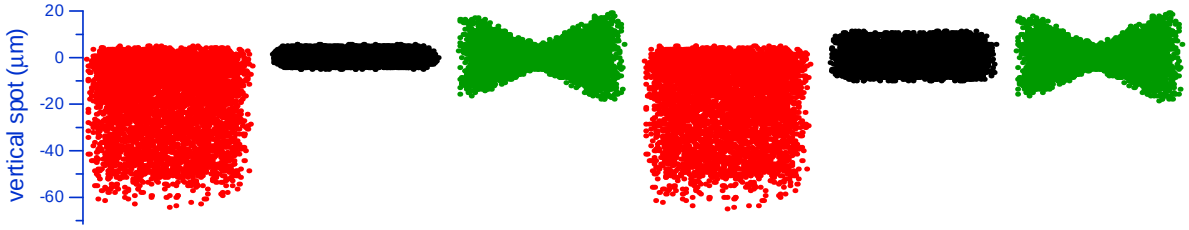

Mirror defects

Slope errors = every deviation from the ideal surface with period larger then ~ 1,2 mm

Typical definition is μrad or arcsec rms.
Alternative definition is λ/10 or λ/20 and so on… P-V or rms
used for normal incidence mirror or "poorer" quality mirrors

Roughness = every deviation from the ideal surface with period smaller then ~ 0.5-1 mm

Typical definition is Å rms.
Alternative definition is surface quality 20-10 or 10-5 (scratch-dig)
used for normal incidence mirror or "poorer" quality mirrors
A dig is nearly equal in terms of its length and width. A scratch could be much longer then width
20-10 means 20/1000 of mm max scratch width 10/100 mm max dig dimension

Roughness

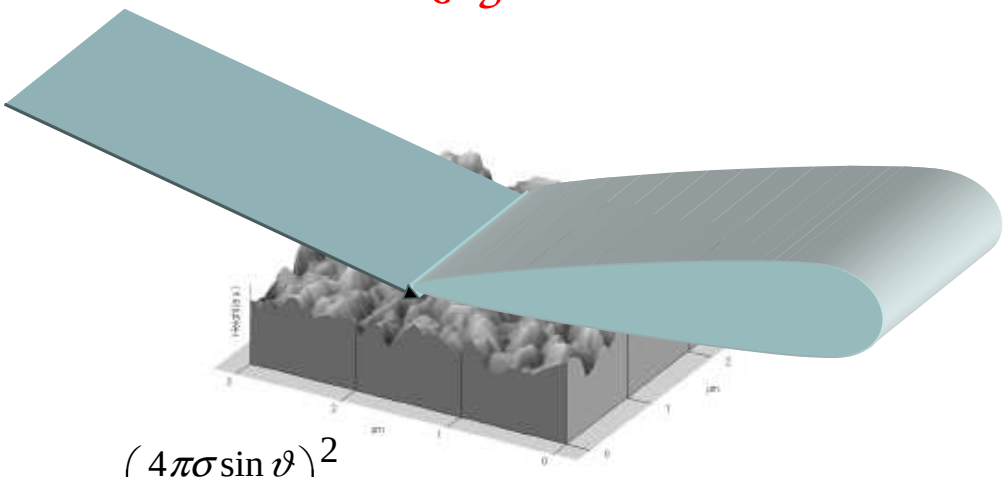

$$I = I_0 e^{-\left(\frac{4\pi\sigma \sin\vartheta}{\lambda}\right)^2}$$

$$\sigma = \sqrt{\frac{1}{n}\sum_{x=0}^{n}\left[s(x) - \overline{s(x)}\right]^2}$$

Roughness

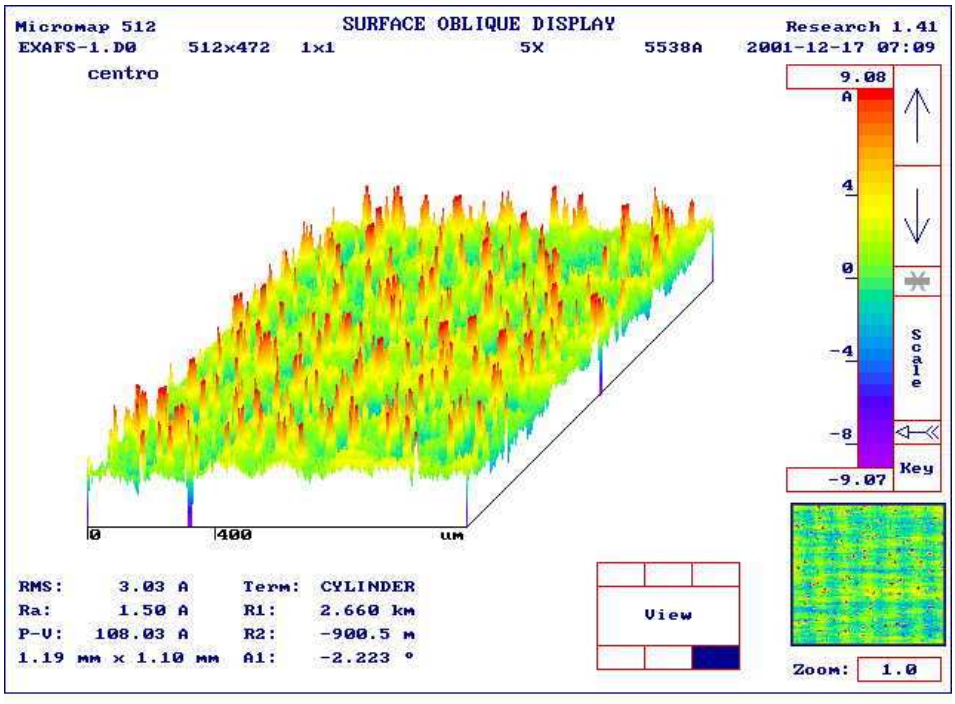

Roughness

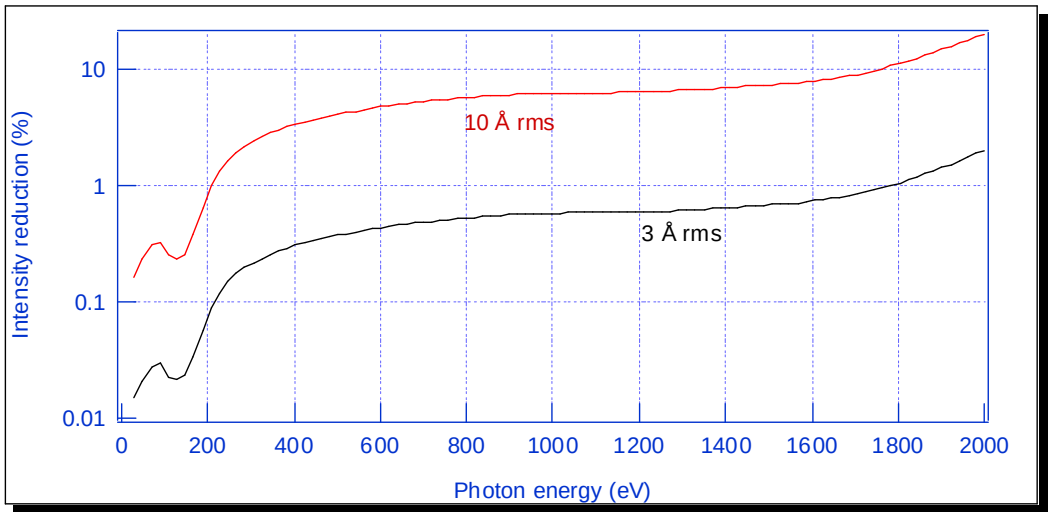

Shape	Spherical/Flat	Toroidal/aspherical
Roughness (Å)	3 standard 1 best	5 standard 3 best

Beamline layout

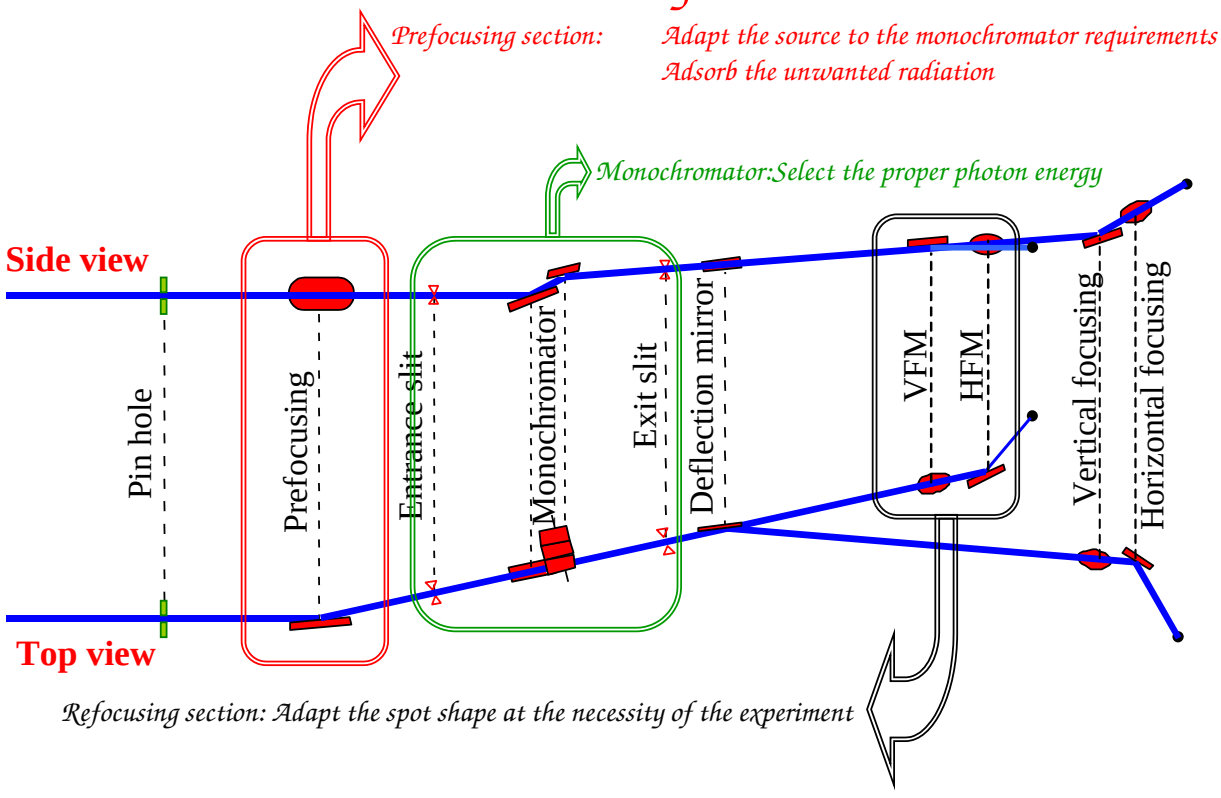

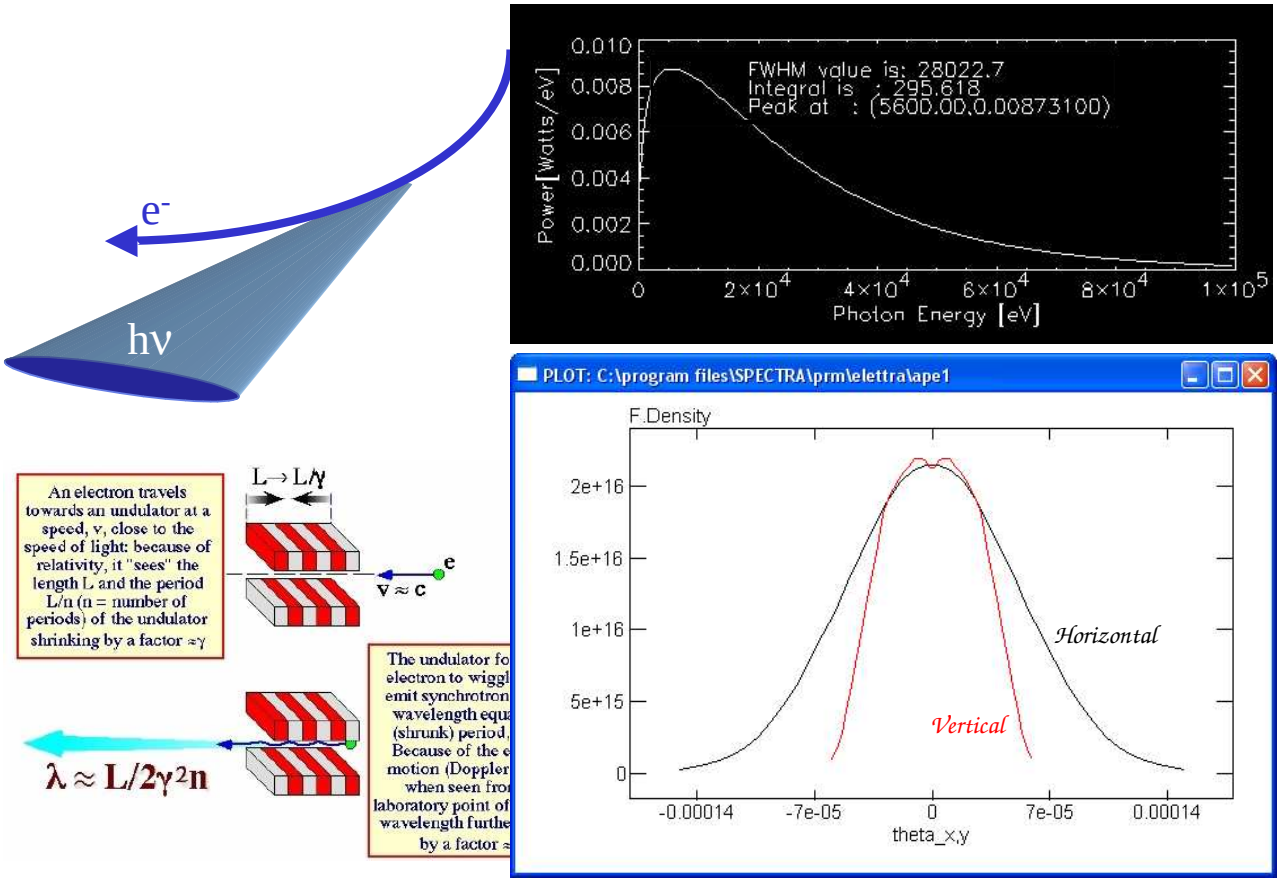

One of the major advantages of Synchrotron Radiation (SR) sources, is their ability to provide high brilliance photons in the soft x-ray region. This part of the electromagnetic spectrum is of great interest, because many materials have strong absorption edges at these energies. If one is able to monochromate these photons, the chemical state of atoms and molecules can be studied in depth, and consequently their interaction behaviour understood.
Unfortunately, from the point of view of the optics, this strong absorption is a disadvantage. As seen previously, the absorption properties of the materials make impossible the use of ordinary normal incidence optics schemes. Therefore one is forced to work in grazing incidence configurations. Mirror reflectivity decreases dramatically with increasing photons energy and incidence angle. For this reason, grazing incidence angles of 2 degrees or lower, are usually adopted by the SR beamline designers.

The main problem is to found a material which could be polished and treated opportunely to produce the required shape with the required precision and in the mean time, this material have to satisfy some requirements. First of all, the materials have to be UHV compatible, have to have a limited thermal expansion (to avoid deformation under the synchrotron radiation beam) have to be rigid enough to do not be deformed by the clamping system and, in many cases, it must be cooled.
Depending on the material chosen, the roughness and the slope errors could be reduced to acceptable values.
Some widely used materials are summarised in the table presented 2 page later.
From this table, it is evident that Silicon Carbide (SiC) is a good material when one need to cool the mirror/grating. It is in fact rigid enough to do not be deformed by the clamping and has a high figure of merit, i.e. a limited thermal expansion together with a good thermal conductivity. It means that with a cooling system made by a cool object put in tight contact with the edge of the optics, it's possible to dissipate the heat induced by the synchrotron radiation light.
Another advantage of its stiffness is the fact that is possible to polish it with a very good surface finishing. It means that the final roughness could be of the order of 0.1nm rms. The same statement is valid for Silicon and glass material in general, while for metal this is not true. As a matter of fact, the metals are typically malleable, and therefore, the friction with the polishing tools produce always some particles of materials, which damage the surface.
If one need to cool the optics, another possible solution is the use of Glidcop, Copper or Molybdenum, but with the option of the internal cooling.
Since we are dealing with metals we are able to weld its. In reality the procedure of welding is a little bit complicated and must be vacuum compatible and is called "braze".
Nevertheless, it is possible to create some channel close to the optical surface inside the blank and let the water circulate inside it. Therefore, even if the thermal conductivity of the material is poorer respect silicon or SiC, the cooling channel are very close to the optical surface and the cooling procedure is efficient too.

Thermal deformation

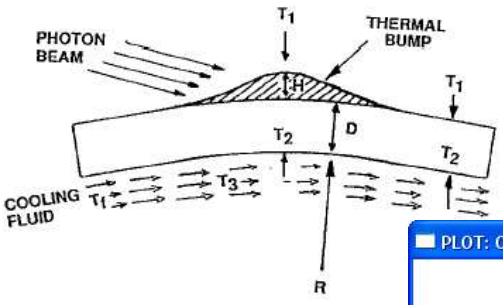

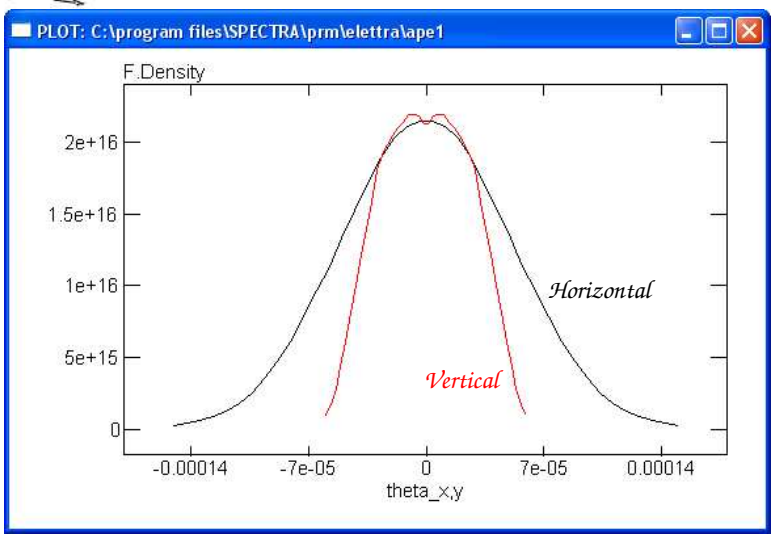

Mechanical and thermal properties of some mirror materials

	Density gm/cc	Young's modulus GPa	Thermal expansion (α) ppm/°C	Thermal conductivity (k) W/m/°C	Figure of merit k/α
Fused silica	2.19	73	0.50	1.4	2.8
Zerodur	2.53	92	0.05	1.60	32
Silicon	2.33	131	2.60	156	60
SiC CVD	3.21	461	2.40	198	82
Aluminum	2.70	68	22.5	167	7.42
Copper	8.94	117	16.5	391	23.7
Glidcop	8.84	130	16.6	365	22
Molybdenum	10.22	324.8	4.80	142	29.6

Side cooling

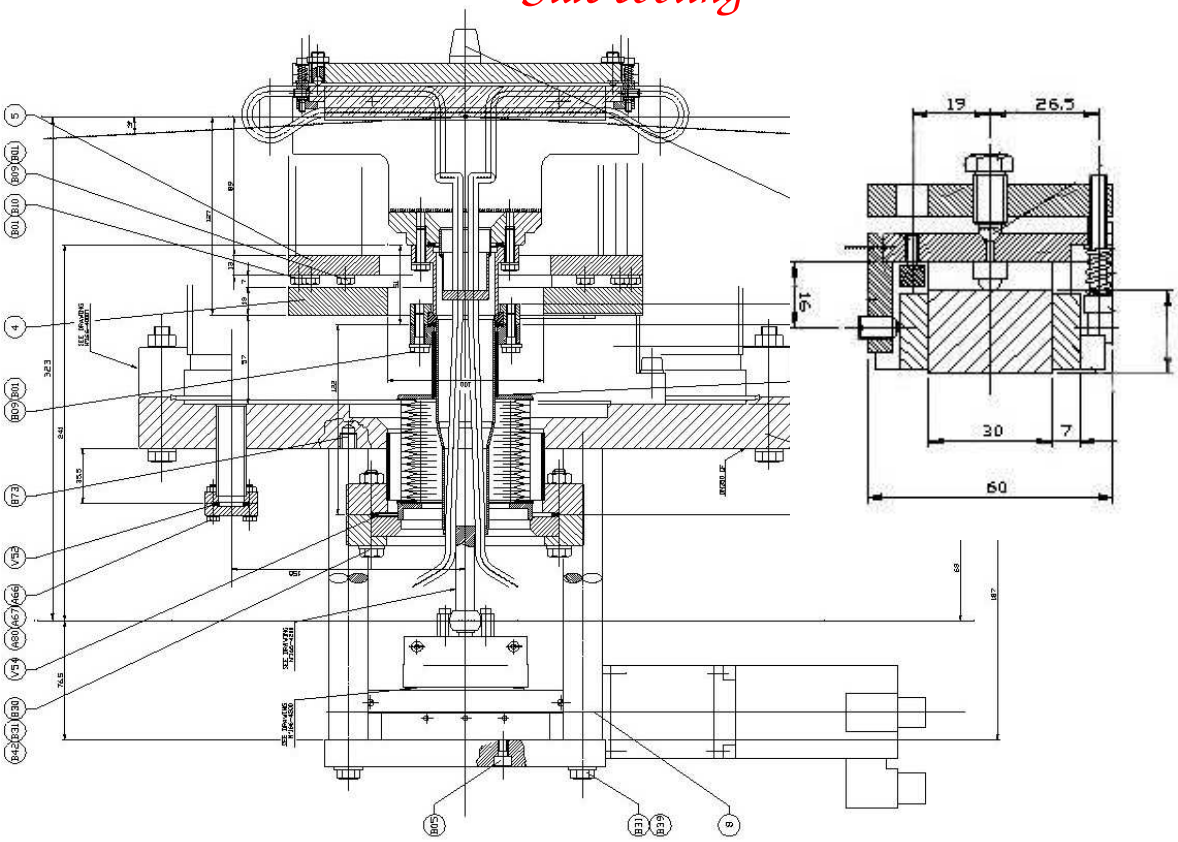

Side cooling

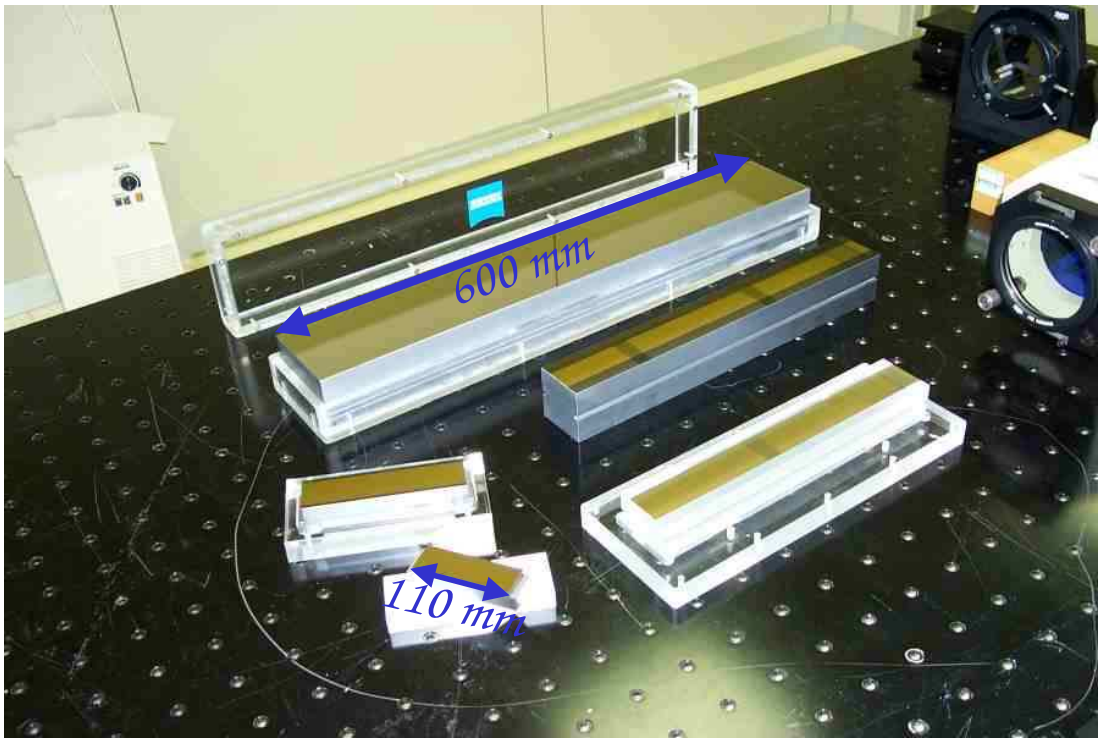

Side cooling

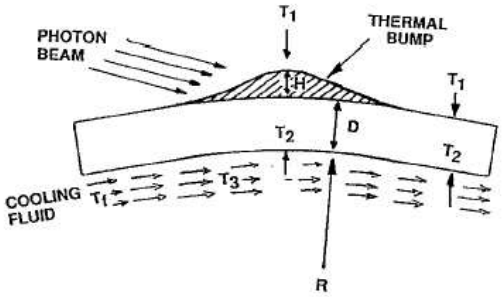

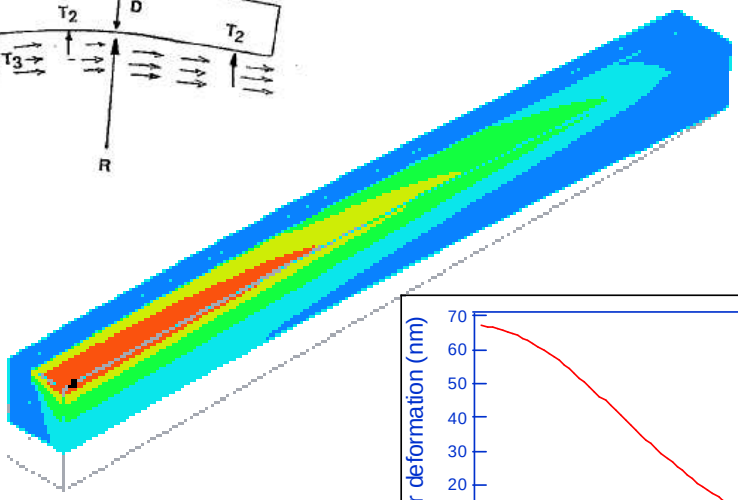

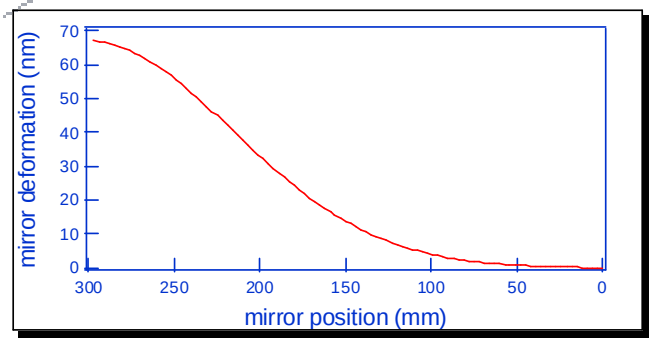

Internal cooling mirror

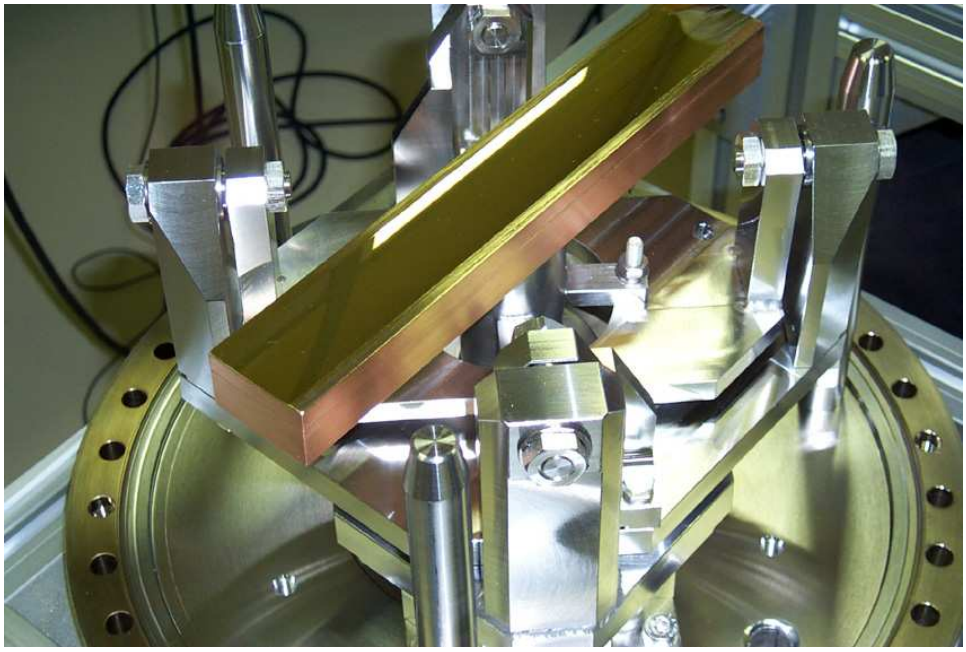

Internal cooling mirror

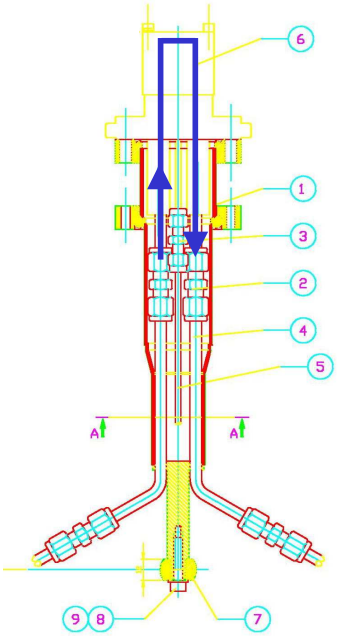

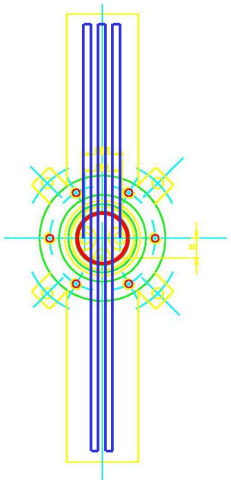

Internal cooling mirror

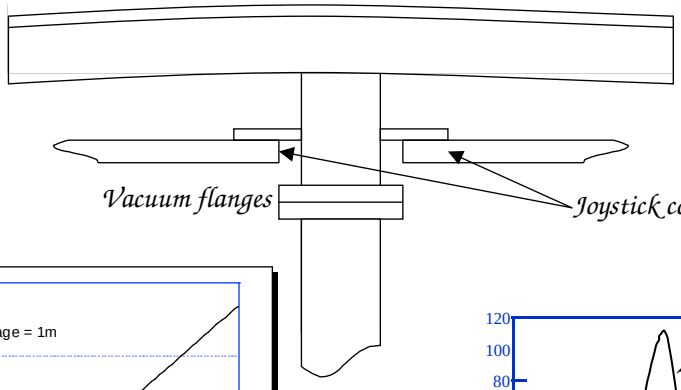

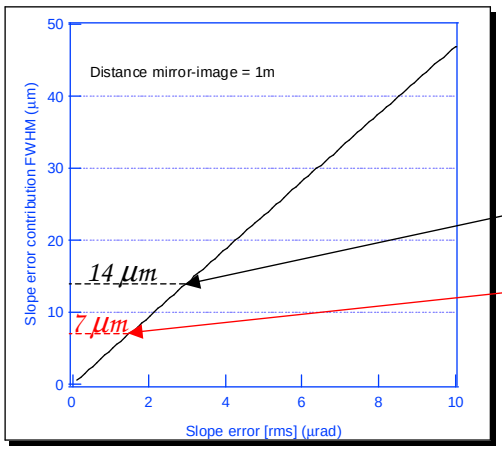

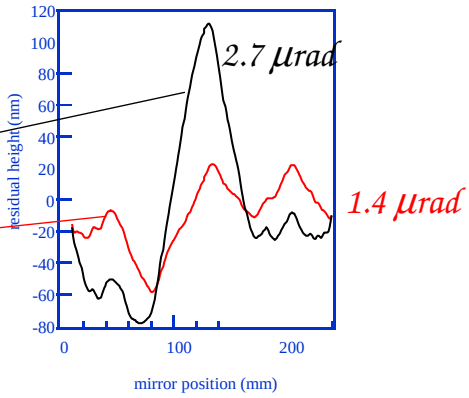

Soft X-ray monochromators

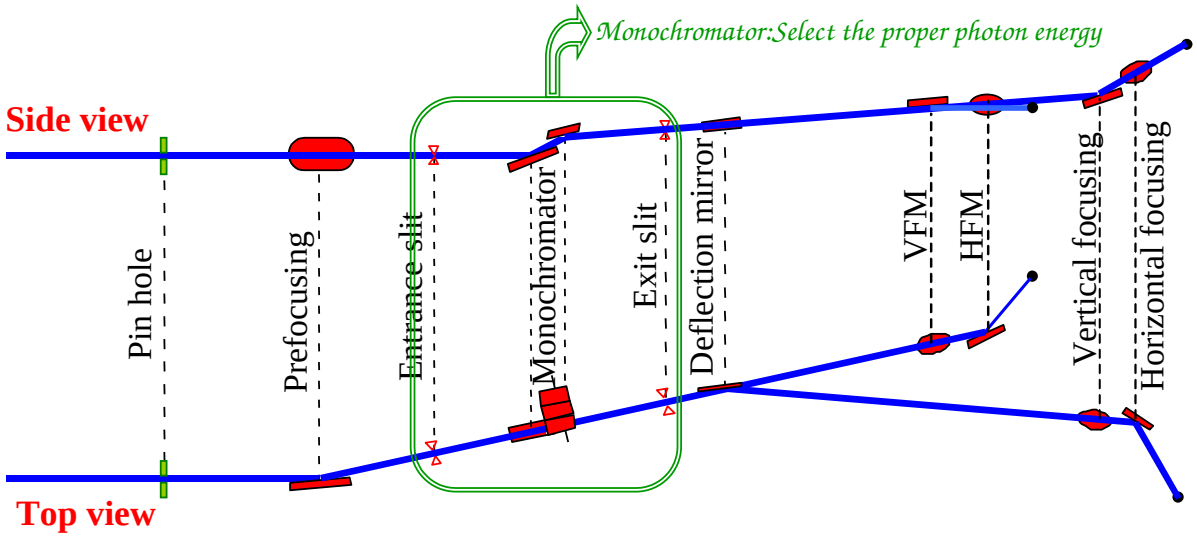

Diffraction grating

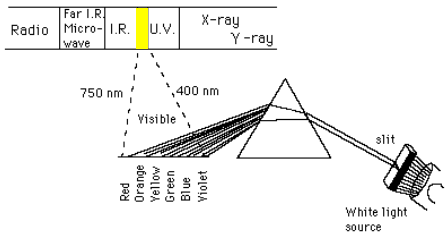

Micro wave	I.R.	Visible	U.V.	Soft X-ray	Hard X-ray

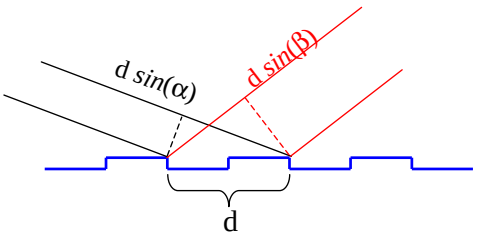

Micro wave	I.R.	Visible	U.V.	Soft X-ray	Hard X-ray

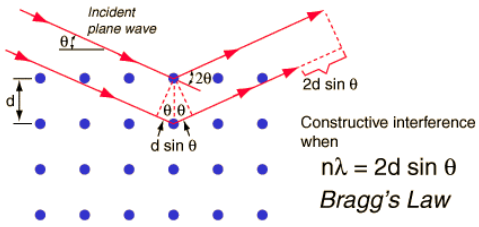

limit ~ 1-2 keV (1 nm)

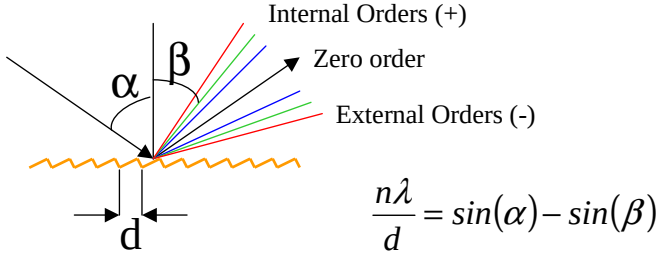

$$\frac{n\lambda}{d} = sin(\alpha) - sin(\beta)$$

Diffraction grating

Gratings

A diffraction grating, the heart of a Soft X-ray beamline, is an artificial periodic structure with a well defined period *d*. Tl incoming and outgoing radiation directions are related by a simple formula:

$$\frac{n\lambda}{d} = sin(\alpha) - sin(\beta) \qquad (1)$$

where α is the angle of incidence and β is the angle of diffraction, both with respect to the normal (see next figure), n tl diffraction order and λ the wavelength of the selected radiation.

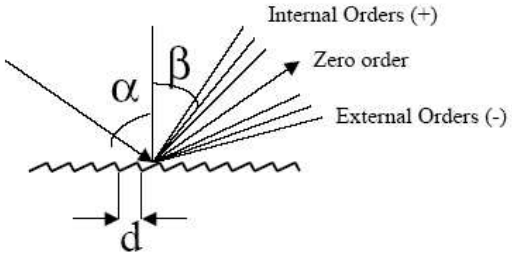

An alternative description of the same law is the following:

$$nK\lambda = sin(\alpha) - sin(\beta) \qquad (2)$$

where K=1/d is the groove density.
The profile of the grooves of the gratings could be sinusoidal (not often used), laminar or blaze.

Diffraction grating

The diffraction gratings can be produced by several ways. They can be mechanically ruled by means of a diamond tool that drills the substrate, holographically recorded and also replicated from a master. In all these cases some errors occur during the manufacturing process. These defects can be periodic (or quasi-periodic) or completely random. In any case, the final effect of these defects is a reduction of the ability of the grating to select the proper photon energy, the reduction of the photon flux (due, for instance, to the stray light) or the presence of unwanted diffracted energy together with the selected one (ghosts). In the next picture, below the rough presentation of the possible imperfections, a formula to estimate the intensity reduction due to the imperfections is reported.

$$I_g = I_0\left(\frac{n\pi\ \delta d}{d}\right)^2 \qquad I = I_0 \exp -\left(\frac{2\pi\ sin\beta\ \delta d}{\lambda}\right)$$

δd is, in the periodic imperfection case, the maximum deviation from the ideal d-spacing, while in the random distributed case is the rms deviation from the ideal d-spacing.
The knowledge of these defects is as important as the knowledge of the slope errors of the substrate of the grating. Typically, people do not specify carefully the groove spacing constancy of the grating or, alternatively, accept a large error because it is very difficult to measure the d-spacing along the whole grating surface with the needed precision.
Nevertheless we can estimate the effect of these errors on the resolving power and on the spot dimension after the grating.
The maximum achievable resolving power could be estimated (after equation 1) by:

$$\frac{\delta\lambda}{\lambda} = \frac{\frac{1}{n}(sin(\alpha) - sin(\beta))\delta d}{\frac{1}{n}(sin(\alpha) - sin(\beta))d} = \frac{\delta d}{d}$$

Diffraction grating

While the minimum spot dimension could be again obtained from equation 1 and is:

$$\delta S = \delta\beta \cdot r' = 2tg\beta \frac{\delta d}{d} r'$$

A different case is the one of the Variable Line Spacing (VLS) grating, where a groove density variation is required. The groove density K(*w*), along the direction *w* perpendicular to the grooves (centred on the pole of the grating), can be described via a polynomial series, i.e.

$$K(w) = K_0 + K_1 w + K_2 w^2 + K_3 w^3 + \cdots \quad (3)$$

One should re-write the optical path function [2] and re-calculate the terms describing the focal property as well as the residual aberrations introduced by the grating. The general expression of these terms is:

$$F_{j00} = \frac{1}{2}\left(-n\lambda K_{j-1} + M_{j00}\right) \quad (4)$$

Where M_{j00} are the terms describing the focal properties and the aberrations of the constant groove density gratings.
It's evident therefore that the polynomial terms K_1, K_2 and so on play a fundamental role in the prediction of the optical behaviour of the VLS gratings. Therefore, the knowledge of these terms is as important as the knowledge of the radius of curvature of a spherical grating or the knowledge of the residual slope errors.
Actually, the state of the art of the grating manufacturing is the following:
The slope errors of the blank could be reduced easily below 0.1 arcsec (0.5 μrad)
The groove density could be made up to 5000 l/mm without too many problems but could be also made larger
The groove density constancy is better then 0.01% (δd/d)
The dimension of an X-ray grating is not larger then 20 cm but typically lower.

Gratings profiles

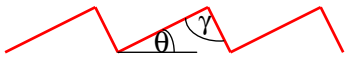

Blaze profile

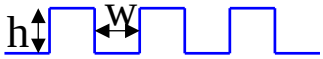

Laminar profile

Blaze gratings: *higher efficiency*

Laminar gratings: *Higher spectral purity*
Higher resolution

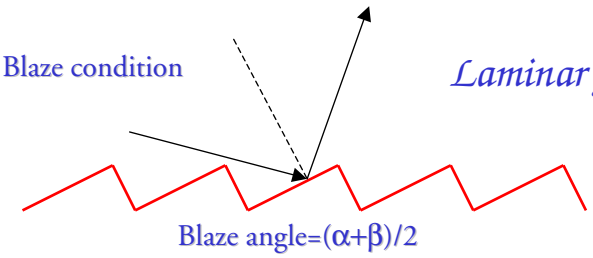

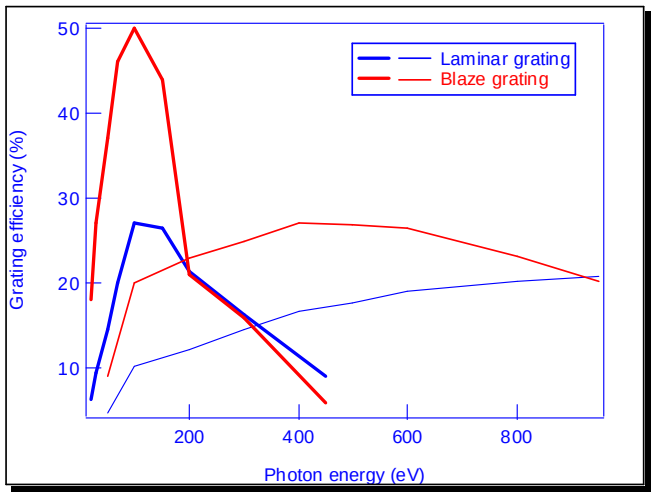

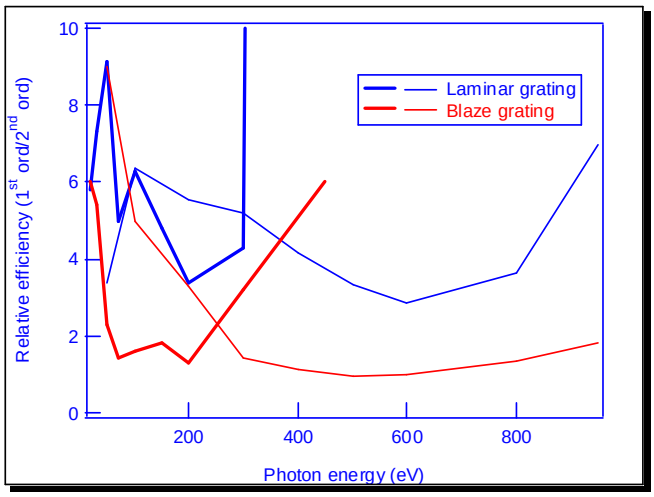

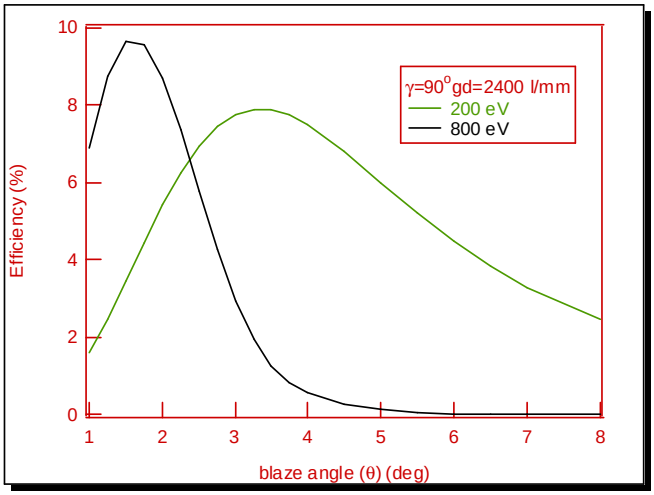

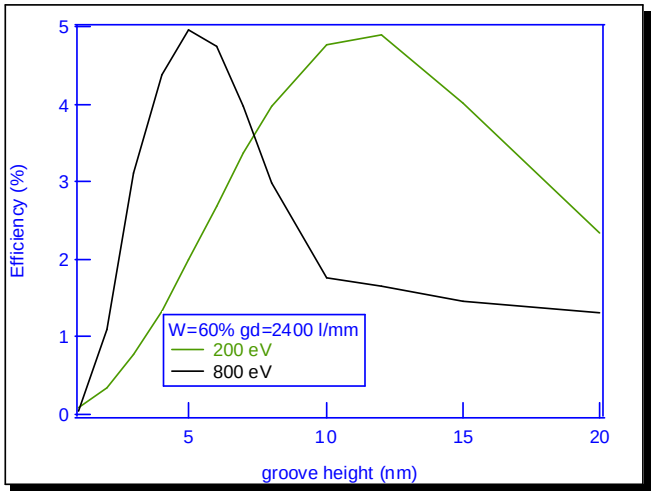

Mechanically ruled grating

Mechanically ruled (CARL ZEISS Grating Ruling Engine GTM6) with blazed profile down to 0.5-0.7°

Mechanical ruling blaze profile → smaller blaze angles; higer efficiency

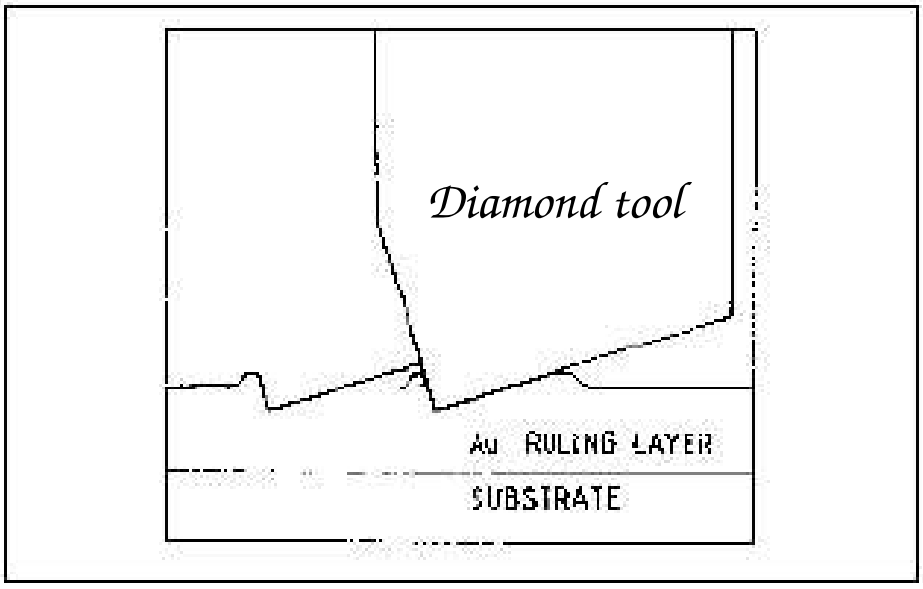

Mechanically ruled grating

Mechanically ruled (CARL ZEISS Grating Ruling Engine GTM6) with blazed profile down to 0.5-0.7°

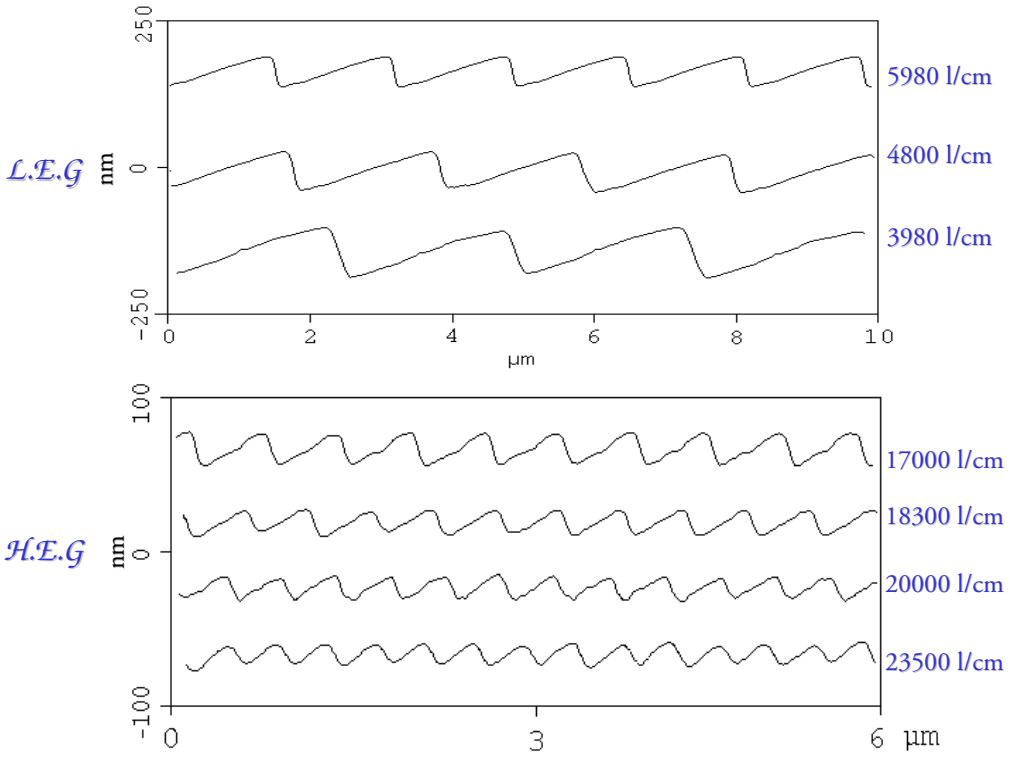

Holographical grating

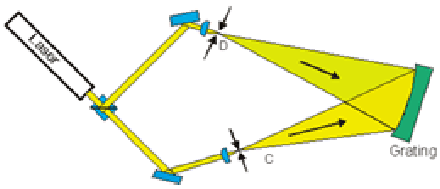

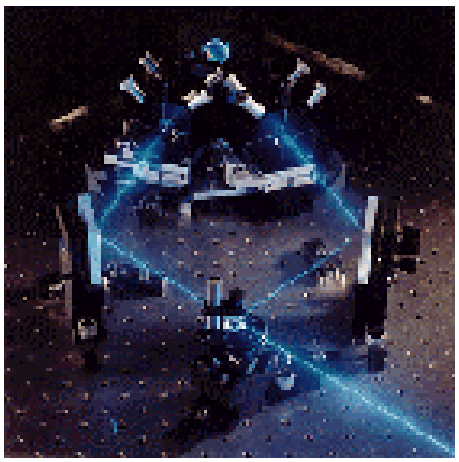

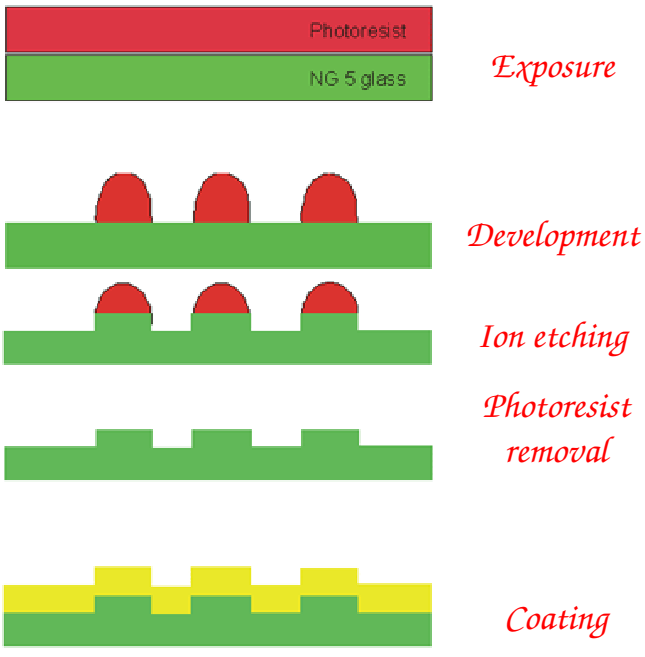

Holographically recording laminar and blaze profile (large blaze angle)

→ higher groove density; lower spacing disomogeneity

Grating's equations

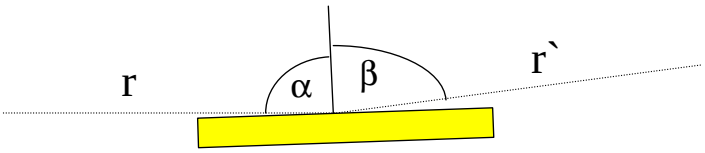

Optical path function

$$F_{100} = -n\lambda D_0 + (\sin\alpha - \sin\beta)$$ *grating equation*

$$F_{200} = \left(\frac{\cos^2\alpha}{r} - \frac{\cos\alpha}{R} + \frac{\cos^2\beta}{r'} - \frac{\cos\beta}{R} \right)$$ *tangential focus*

$$F_{300} = \left[\left(\frac{\cos^2\alpha}{r} - \frac{\cos\alpha}{R} \right) \frac{\sin\alpha}{r} + \left(\frac{\cos^2\beta}{r'} - \frac{\cos\beta}{R} \right) \frac{\sin\beta}{r'} \right]$$ *primary coma*

Rowland condition

$\mathcal{F}_{200} = \mathcal{F}_{300} = 0$

$r = \mathcal{R}\cos\alpha$

$r' = \mathcal{R}\cos\beta$

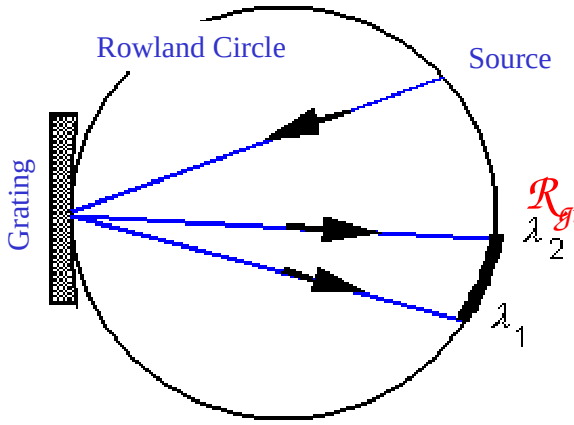

$\mathcal{R}_{grating} = 2\mathcal{R}_{rowland\ circle}$

$$F_{200} = \left(\frac{\cos^2\alpha}{r} - \frac{\cos\alpha}{R} + \frac{\cos^2\beta}{r'} - \frac{\cos\beta}{R} \right)$$ *tangential focus*

$$F_{300} = \left[\left(\frac{\cos^2\alpha}{r} - \frac{\cos\alpha}{R} \right) \frac{\sin\alpha}{r} + \left(\frac{\cos^2\beta}{r'} - \frac{\cos\beta}{R} \right) \frac{\sin\beta}{r'} \right]$$ *primary coma*

Plane/spherical grating monochromators

$$F_{100} = -n\lambda D_0 + (\sin\alpha - \sin\beta)$$

$$F_{200} = \left(\frac{\cos^2\alpha}{r} - \frac{\cos\alpha}{R} + \frac{\cos^2\beta}{r'} - \frac{\cos\beta}{R} \right)$$

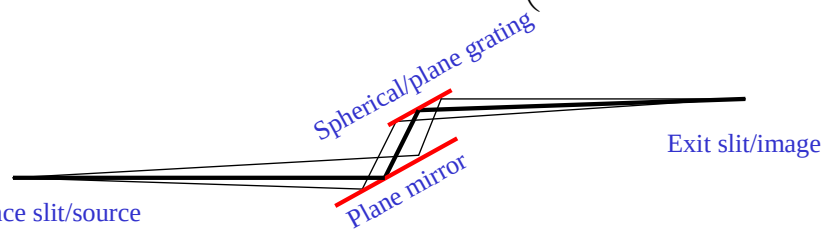

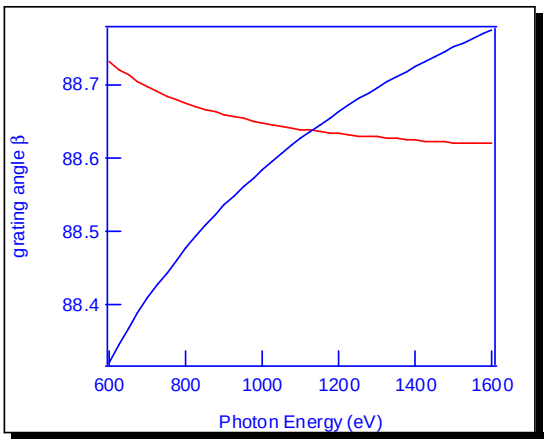

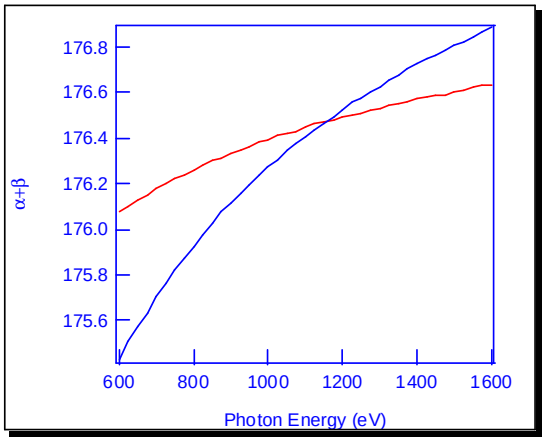

Resolving power

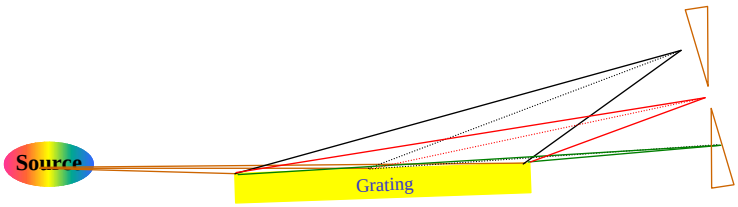

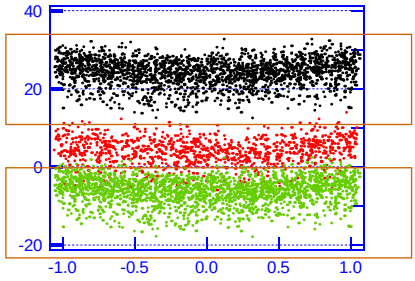

Exit slit

Note: the angula precision of the grating rotation have to allow the energy selection i.e. 0.2-0.3 μrad

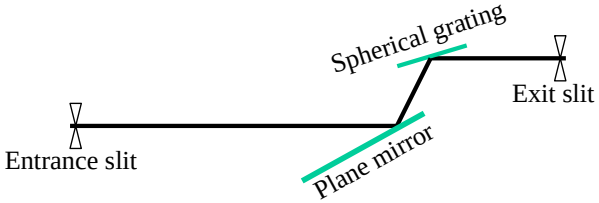

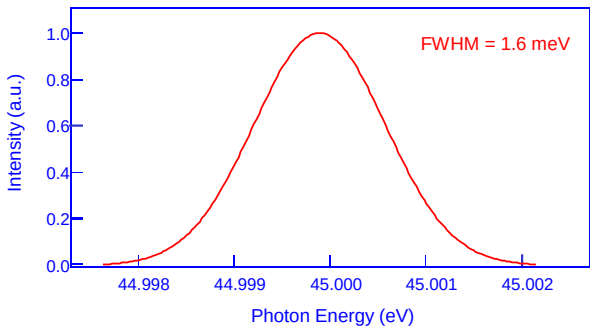

$$N k \lambda = \sin(\alpha) - \sin(\beta)$$

$$\left(\frac{\partial\lambda}{\partial\alpha}\right) = \frac{\cos(\alpha)}{Nk} \qquad \Delta\alpha = \frac{s}{r} \qquad \Delta\lambda_{entrance} = \frac{s \cdot \cos(\alpha)}{Nkr}$$

entrance slit contribution

$$\left(\frac{\partial\lambda}{\partial\beta}\right) = \frac{\cos(\beta)}{Nk} \qquad \Delta\beta = \frac{s'}{r'} \qquad \Delta\lambda_{exit} = \frac{s' \cdot \cos(\beta)}{Nkr'}$$

exit slit contribution

Resolving power

Typical Spherical grating monochromator resolving power

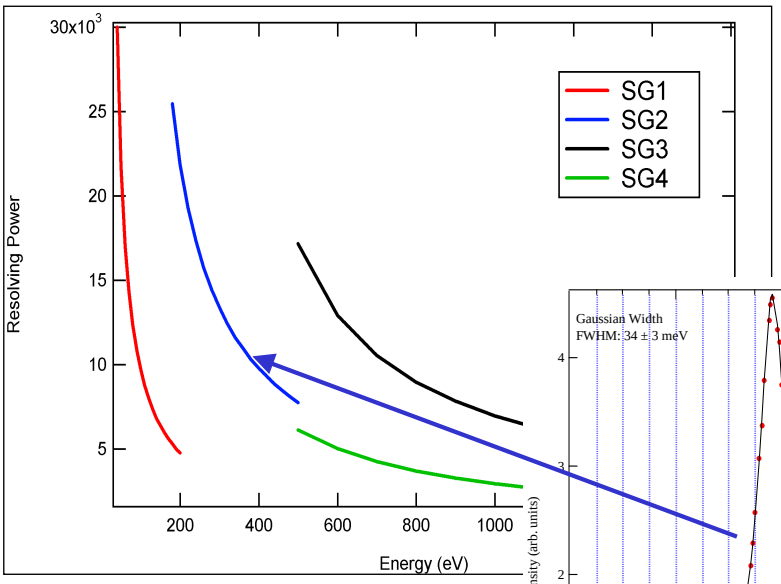

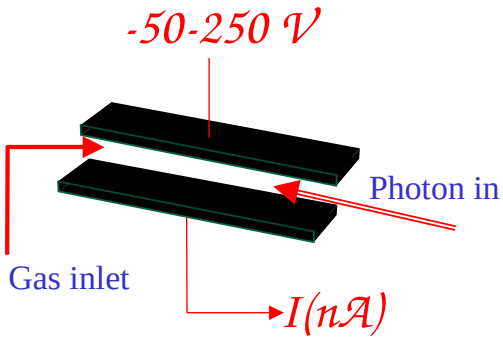

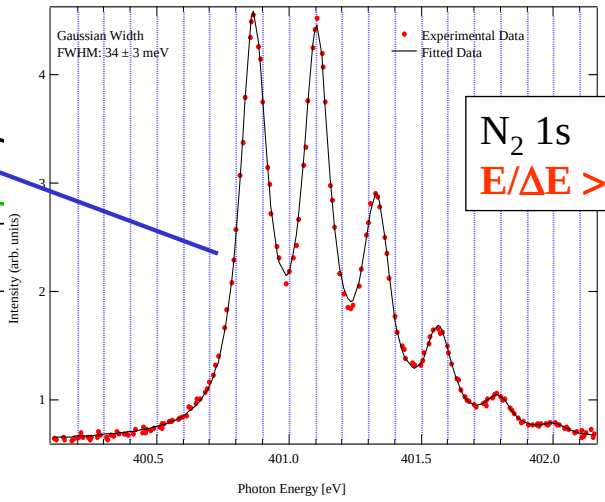

N_2 1s

E/ΔE > 11000

Resolving power

Typical Spherical grating monochromator resolving power

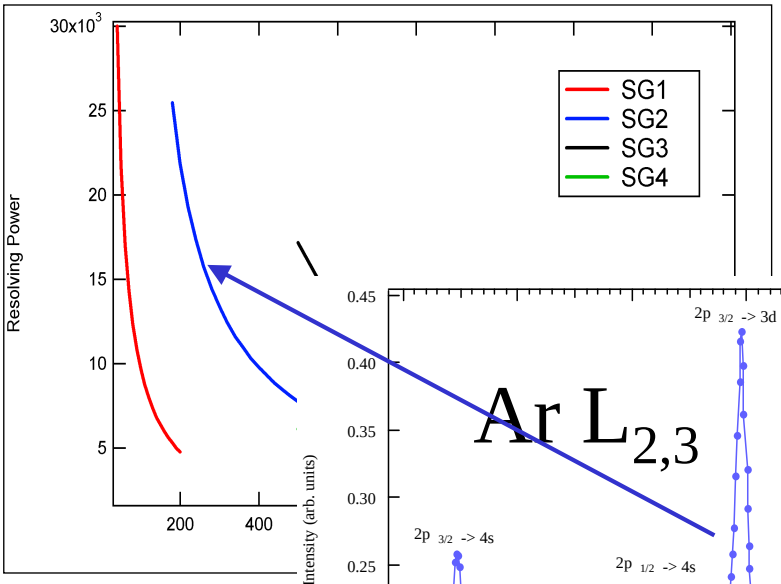

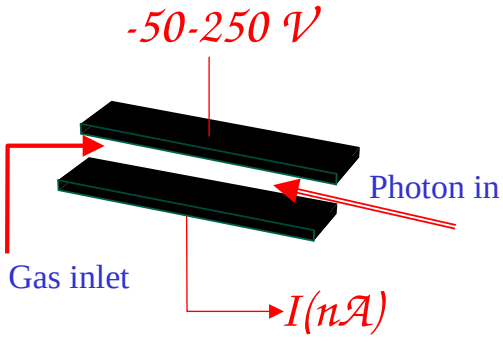

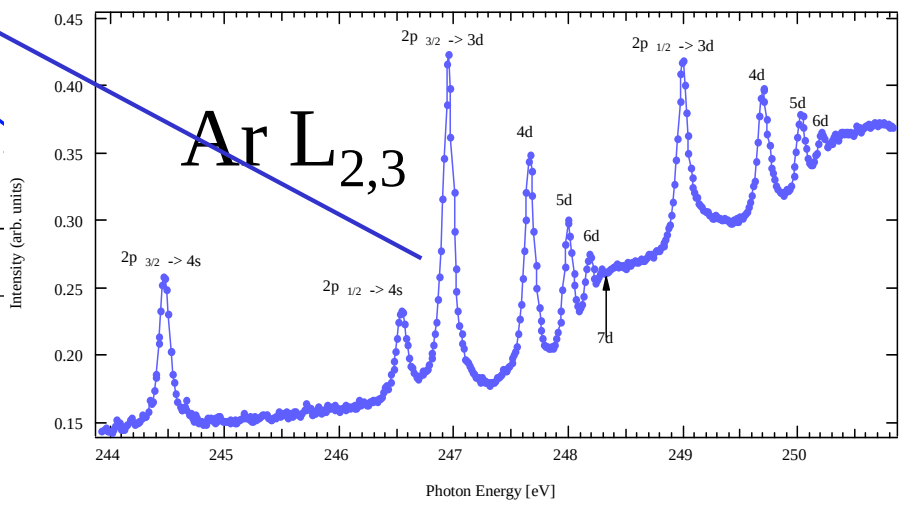

Magnification

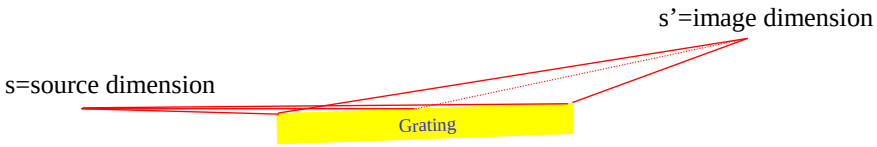

$$M(\lambda)=\frac{s'}{s}$$

$$Nk\lambda = sin(\alpha)-sin(\beta) \Rightarrow \begin{cases} \left(\frac{\partial\lambda}{\partial\alpha}\right)=\frac{\cos(\alpha)}{Nk} & \Delta\alpha=\frac{s}{r} \\ \left(\frac{\partial\lambda}{\partial\beta}\right)=\frac{\cos(\beta)}{Nk} & \Delta\beta=\frac{s'}{r'} \end{cases}$$

$$M(\lambda)=\frac{s'}{s}=\frac{r'\ \cos(\alpha)}{r\ \cos(\beta)}$$

Variable line space grating

Groove density D varies along the grating surface: $\mathcal{D}(x)=\mathcal{D}_0+\mathcal{D}_1 x+\mathcal{D}_2 x^2+\mathcal{D}_3 x^3+\cdots$

$$\mathcal{F}_{200}=\frac{1}{2}\left(-n\lambda\mathcal{D}_1+\left(\frac{cos^2\alpha}{r}-\frac{cos\alpha}{\mathcal{R}}+\frac{cos^2\beta}{r'}-\frac{cos\beta}{\mathcal{R}}\right)\right)$$

$$\mathcal{F}_{300}=-\frac{1}{3}n\lambda\,\mathcal{D}_2+\frac{1}{2}\left[\left(\frac{cos^2\alpha}{r}-\frac{cos\alpha}{\mathcal{R}}\right)\frac{sin\alpha}{r}+\left(\frac{cos^2\beta}{r'}-\frac{cos\beta}{\mathcal{R}}\right)\frac{sin\beta}{r'}\right]$$

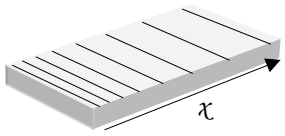

$$\mathcal{F}_{M00}=-c_M n\lambda\,\mathcal{D}_M+\mathcal{K}_{M00}$$

Reduction of higher order aberrations

Focusing plane gratings

Constant demagnification ratio of plane VLS monochromators

Increasing of focusing property of spherical gratings

ComIXS; a compact soft x-ray spectrometer

Soft X-ray Emission Spectroscopy (SXES) is a potentially powerful method to investigate materials that are difficult or impossible with electron spectroscopy. The applicability of this technique ranges from industrial research to basic science due to its elemental and chemical state specificity. The technique is based on the collection, energy selection and counting of the photons emitted by an irradiated sample. The collection of photons instead of electrons permits the application of this technique to insulator or semiconductor materials, as well as use in the presence of strong magnetic fields. The probing depth is larger for the photons (tens to hundreds of nm) than for electrons (few nm), so that SXES is intermediate between surface techniques like electron spectroscopy and bulk techniques like X-ray diffraction, which can be an advantage for interface or thin film studies.

The obstacle to more widespread use of SXES is the low count-rate. First of all, the efficiency of the x-ray emission (i.e. fluorescence) is quite low, especially for low energy transitions. Secondly, to extract useful information from the scattered photons, it is necessary to energetically analyze them, so that a soft x-ray spectrometer should be used, which generally has low efficiency.

The main characteristic of a spectrometer must therefore be to maximize angular acceptance (to collect as many photons as possible), the optical throughput and the detection efficiency. The basic concept is to have as few optical elements as possible (possibly only one, a diffraction grating) with the maximum possible efficiency. Another constraint we imposed was to make the spectrometer as compact and simple as possible, but with the possibility to have a relatively high energy resolving power. The compactness constraint is important to allow the installation of the instrument on different experimental chambers without exotic solutions, and to simplify the alignment procedure and mechanical design.

The solution we adopted is based on the use of two interchangeable Variable Line Spacing (VLS) spherical gratings and is an evolution of the original designs of Nordgren and Calcott. The general layout of the spectrometer is presented in this figure

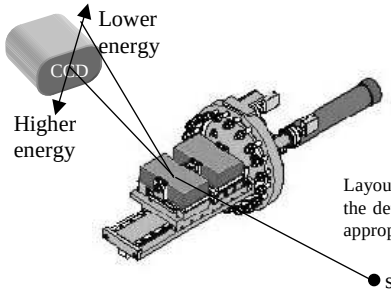

Layout of ComIXS[8]. The two interchangeable gratings are fixed (with respect to the source) while the detector (a back illuminated CCD) moves along a straight line of roughly 6 cm to select the appropriate energy window.

To keep the mechanics of the instrument as simple as possible, the grating is fixed (angle of incidence α and source distance r constant for each energy) and the detector moves to change the energy.

The radius of curvature R of the gratings was chosen to satisfy the first part of the Rowland condition for each energy i.e $R=r/\cos(\alpha)$. Making this choice, and using a grating with a groove density $D(x)$ which varies along the grating as a polynomial function $D(x) = D_0 + D_1x + D_2x^2 + \cdots$ (the origin is the pole of the grating) the equation describing the focal property of the grating becomes:

$$F_{200} = \frac{1}{2}\left(- n\lambda D_1 + \left(\frac{\cos^2 \beta}{r'} - \frac{\cos \beta}{R} \right) \right)$$

In this way the parameter r' (focal distance of the grating) at a particular wavelength λ assumes different values depending on the groove density variation parameter D_1. We select D_1 in such a way that the focal positions of the grating at different energies were as close as possible to a straight line. In this way there is a considerable simplification of the mechanics necessary to select the energy and all the photon energies collected by the detector are in focus.

In principle it is possible to cover the full energy range (≈25-1000 eV) with a single grating, but to reduce the overall displacement of the detector and to increase the efficiency, we used two blazed gratings. For the reason explained above, they have the same radius of curvature (1432.7 cm) the same sample-grating distance (63 cm) and grazing angle of incidence (2.52°). The groove densities and the groove density variations differ by a factor four. In this way, where the low energy grating focuses a particular energy, the other focuses an energy four time larger. To fulfil the above-mentioned requirements, it is necessary that the two gratings have a very large groove density variation. The low energy grating (25-300 eV) has a groove density ranging from 4000 to 6000 l/cm while the high energy one (100-1000eV) from 16500 to 23000 l/cm (with D_0=19200 l/cm and D_1=800 l/cm^2). The required groove density variation for the high energy grating is very difficult to achieve with holographic techniques, therefore mechanical ruling was used as manufacturing process. The grating was ruled using the CARL ZEISS Grating Ruling Engine GTM6, which is operated under interferometric control. It enables one to rule variable line density gratings with a wide range of parameters. Normally, the mechanical ruling is done under a lubricant protection. In the present case a 'dry' ruling technique was used, especially developed for the manufacturing of synchrotron gratings, to reduce considerably molecular contamination.

The groove density variation was tested by measuring the autocollimation angle α_n defined by the equation : $2\sin(\alpha_n) = n\lambda D$ at different diffraction orders n in several grating positions. For a constant groove density grating, the expected relative error in the groove density determination ($\delta D/D$) is lower than 10^{-5}. However, in the case of large groove density variation and high groove density, there is a large spread of the diffracted beam and an enlargement of the diffracted spot (about 1 mm in this case). This reduces the accuracy in the determination of the relative error to 10^{-4}. This is the main limiting factor in the quality control of VLS-gratings.

With these two gratings, all the energies lie on a curve (visible in the next pages) that is not exactly a straight line, but close to it. The maximum difference along the photon path between the straight line and the real focal curve is of the order of 2 mm over the full energy range. The divergence of the radiation is small enough not to enlarge appreciably the spot collected out of its ideal focus.

The closeness of the detector to the grating and to the sample offers two important advantages: a large angular acceptance (26x6 mrad^2 (limited by the CCD width in horizontal)) and a large energy range collected in a single image (of the order of ± 50% of the central selected energy).

The spectrometer is well matched to the beamline BACH at Elettra which hosts it. The beamline delivers monochromatic photons (of the order of 10^{11}-10^{12} ph/sec) in a very small spot (about 12μm in the vertical direction). In this way, the spot becomes the source of the spectrometer without the necessity to adopt an entrance slit. The incoming light can be polarized linearly (horizontal and vertical) or elliptically (including circularly), permitting the performance of inelastic dichroic X-ray scattering experiments.

With such a small spot in the experimental chamber, and with the used gratings, in principle the energy resolution can be very high (up to 30000 at the lower energies). In practice, the actual resolution (measured to be above 1000 in most of the range) is mainly limited by the detector used. Due to the low expected count-rate, an exit slit and single counting system is not suitable, so that a position sensitive detector must be chosen. The energy of a photon is associated with a position in space recorded by the detector. The ideal detector is one with good spatial resolution (much smaller than the dimension of the diffracted image) and the highest possible efficiency together with very low noise. We used a back illuminate CCD (made by Princeton Instruments) mounted perpendicularly to the incoming radiation (a configuration which maximizes the efficiency and permits us to have all of the active surface usable). The CCD has a pixel size of 20X20 μm^2.

Spherical VLS spectrometer (ComIXS)

Groove density D varies along the grating surface: $\mathcal{D}(x)=\mathcal{D}_0+\mathcal{D}_1 x+\mathcal{D}_2 x^2+\mathcal{D}_3 x^3+\cdots$

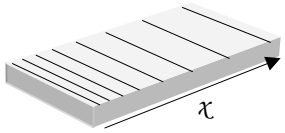

$$\mathcal{F}_{200}=\frac{1}{2}\left(-n\lambda\mathcal{D}_1+\left(\frac{\cos^2\alpha}{r}-\frac{\cos\alpha}{\mathcal{R}}+\frac{\cos^2\beta}{r'}-\frac{\cos\beta}{\mathcal{R}}\right)\right)$$

$$\mathcal{F}_{300}=-\frac{1}{3}n\lambda\,\mathcal{D}_2+\frac{1}{2}\left[\left(\frac{\cos^2\alpha}{r}-\frac{\cos\alpha}{\mathcal{R}}\right)\frac{\sin\alpha}{r}+\left(\frac{\cos^2\beta}{r'}-\frac{\cos\beta}{\mathcal{R}}\right)\frac{\sin\beta}{r'}\right]$$

If distance source-grating and angle of incidence are kept constant i.e. $\mathcal{R}=\frac{r}{\cos\alpha}$

$$\mathcal{F}_{200}=\frac{1}{2}\left(-n\lambda\mathcal{D}_1+\left(\frac{\cos^2\beta}{r'}-\frac{\cos\beta}{\mathcal{R}}\right)\right)=0 \Longrightarrow r'=f\left(\beta(\lambda),\mathcal{D}_1\right)$$

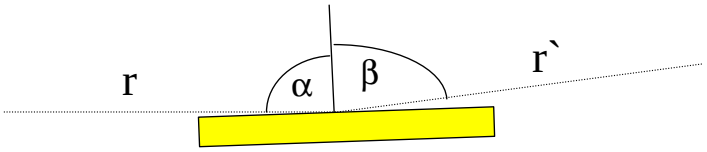

Spherical VLS spectrometer (ComIXS)

$$\mathcal{F}_{200}=\frac{1}{2}\left(-n\lambda\mathcal{D}_1+\left(\frac{\cos^2\beta}{r'}-\frac{\cos\beta}{\mathcal{R}}\right)\right)$$

D_0=19200 l/cm
r=63 cm
R≈14 m

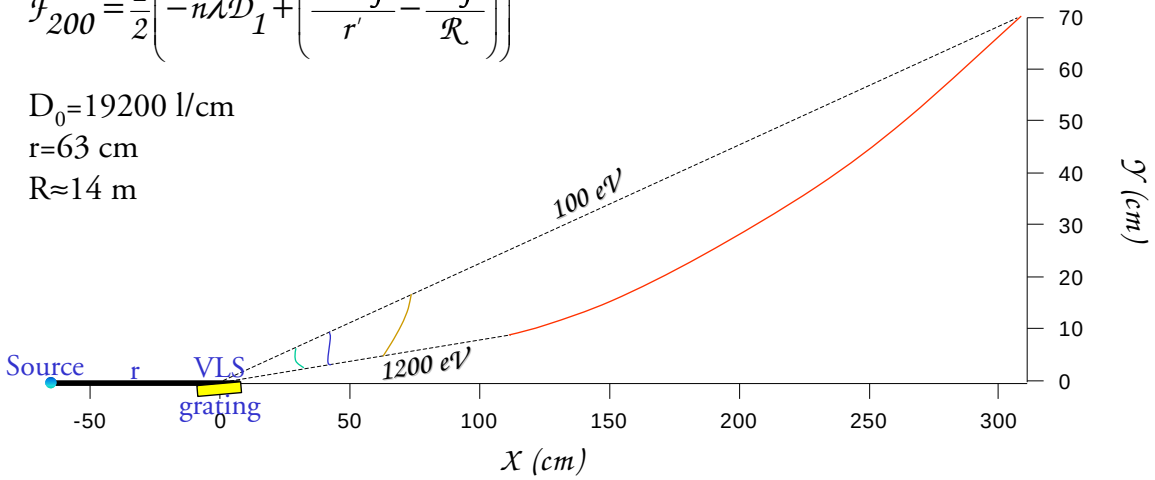

D_1=0 D_1=400 l/cm² D_1=800 l/cm² D_1=1200 l/cm²

Compact Inelastic X-ray spectrometer

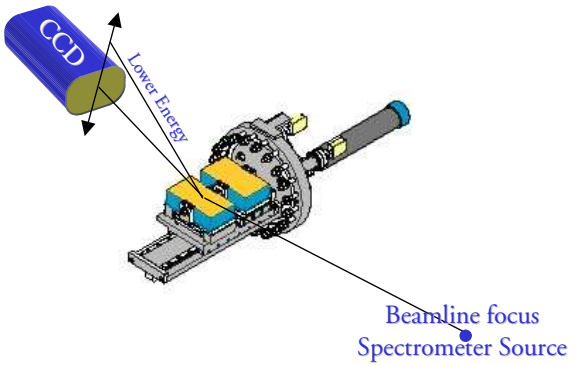

Distance sample grating (cm)	63	
Distance grating CCD (cm)	variable ≈ 42	
Angle of incidence(deg)	87.48	
radius of curvature (cm)	1432.7	
	LEG	HEG
Energy range (eV)	25-200	100-1200
$\mathcal{D}_0$ (l/cm)	4800	19200
$\mathcal{D}_1$ (l/cm^2)	200	800
$\mathcal{D}_2$ (l/cm^3)	7.5	30

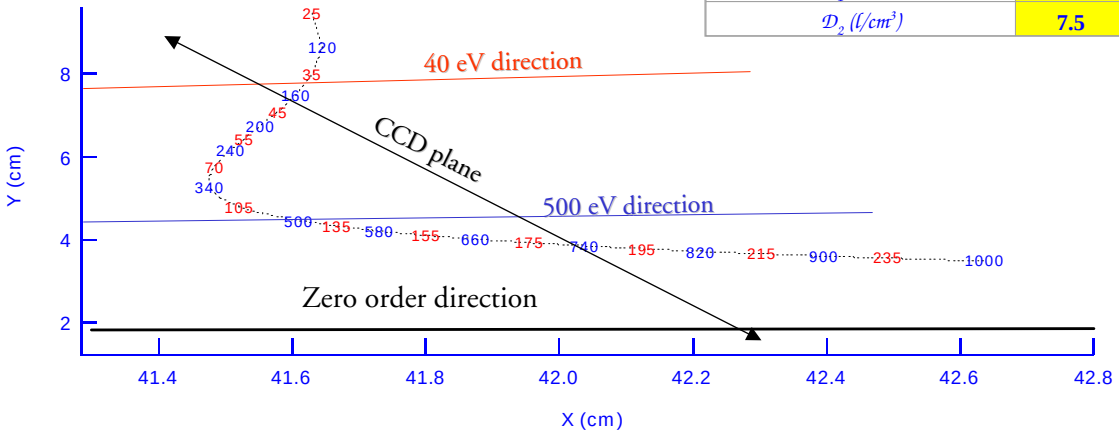

Focal position of the spectrometer as a function of energy. The numbers on the curve indicate the energy focused by the LEG (red) or the HEG (blue). The lower black line indicates the direction of zero order, which is accessible. The direction of the diffracted radiations and the CCD plane are also displayed. The origins of X and Y are the pole of the grating.

Spherical Variable line space grating

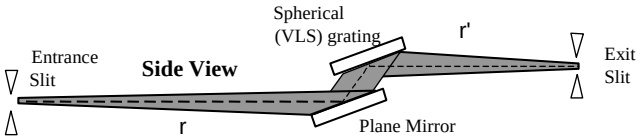

$$\mathcal{F}_{300} = -\frac{1}{3}n\lambda\,\mathcal{D}_2 + \frac{1}{2}\left[\left(\frac{\cos^2\alpha}{r} - \frac{\cos\alpha}{\mathcal{R}}\right)\frac{\sin\alpha}{r} + \left(\frac{\cos^2\beta}{r'} - \frac{\cos\beta}{\mathcal{R}}\right)\frac{\sin\beta}{r'}\right]$$

200eV

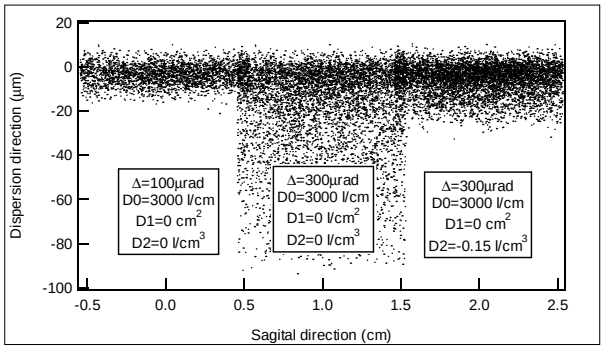

70eV

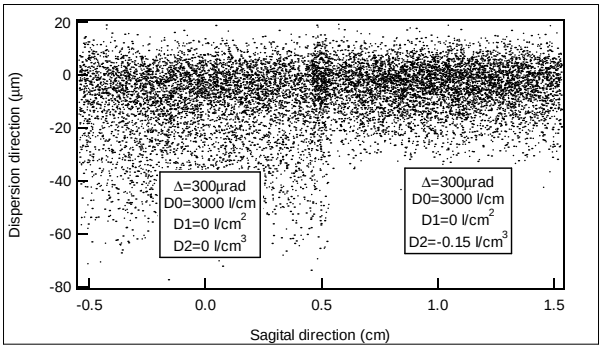

The Nanospectroscopy beamline at Elettra is used to probe the electronic and magnetic properties of surfaces and interfaces at the nanometer length scale. For this purpose, the beamline serves two end stations, equipped with high lateral resolution direct imaging X-ray microscopes. The beamline first branch, operational since fall 2002, hosts the SPELEEM microscope (Spectroscopic Photoemission and Low Energy Electron Microscope). In order to to achieve high spatial resolution and maximise the collection efficiency, the beamline was designed to convey the highest possible flux density at the microscope focus. Target requirements were met by combining an insertion device with a moderate energy resolving power monochromator, together with careful refocussing of the photon beam. Given the typical working conditions of the microscope (few µm to 10 µm field of view), the beamline strongly demagnifies the source, providing homogeneous illumination of the sample area which is imaged by the microscope.

The Nanospectroscopy beamline shares the photon source with the Elettra Free Electron Laser (FEL). The source consists of two identical Sasaki Apple II type undulators, each with 20 periods of 10 cm length, coupled by a phase modulation electromagnet. The source is able to provide elliptically polarised light (circular left and right as well as linear horizontal and vertical as special cases) in a spectral range extending from 10 eV to 1000 eV, with high brilliance (using the first, third and fifth undulator harmonic). The source size FWHM at 400 eV is 560 µm in the horizontal and 50 µm in the vertical.

The layout of the beamline is shown in the next slide. The first mirror encountered by the radiation is toroidal, 16 m from the source. The mirror has two different focal positions for the horizontal and vertical direction which correspond to two different slits, one for the horizontal focus (2 m behind the mirror) and one for the vertical (3 m behind the mirror). The vertical slit becomes the source for the monochromator. The toroidal mirror accepts a high flux of photons and absorbs a large heat load. In order to reduce heat induced deformation, the mirror, made from glidcop, has got internal water cooling. The main advantage of internal with respect to side cooling is the closeness of the water circulating tubes to the optical surface (between 1 and 3 mm). The mirror was designed and developed by the Elettra mechanical engineering group.

The beamline monochromator is based on a Variable Line Space (VLS) plane grating. With a plane VLS grating, one can cover a large energy range with a relatively small change in the resolving power. As shown on the Plane VLS slide, the VLS architecture allowed us to use only two gratings for the range from 20 eV to 1000 eV. This wide range can be covered only if the angle between incident and diffracted beam can change. This is achieved with a plane mirror in front of the grating. By coupling the rotation of mirror and grating, the beam can always be diffracted in the desired direction. The first grating has 200 l/mm and covers the energy range from 20 to 250 eV, while the second grating (400 l/mm) covers the range from 200 to 1000 eV.

After the monochromator, there is the refocusing section. The goal is to obtain a homogeneous microspot which provides the highest possible photon flux within the field of view of the microscope. This requires a very strong demagnification. To reach this goal, each of the two beamline branches hosts two bendable plane elliptical mirrors mounted in a Kirkpatrick-Baez (KB) configuration. The surface profile of bendable mirrors can be finely controlled by applying unequal end-moments to the mirror body. Elliptical profiles can be approximated with high accuracy, enabling to change the focal distance of the mirror. A spot size of 6 µm (hor.) x 2 µm (vert.) FWHM has been calculated for the mirrors of the SPELEEM branch at photon energy 140 eV and 10 µm exit slit.

The alignment of the KB mirrors and the optimization of the mirror bender settings was done by minimizing the size of the beam image on the sample. An image shown in the next slides has been acquired with the SPELEEM. The possibility to dynamically optimize the mirrors while monitoring the focal spot has been essential for producing the best optical focus. A slide shows the optimized double focused beam, with horizontal and vertical line profiles which give 7 µm x 2 µm FWHM. These profiles are already corrected for the 16° grazing incidence angle of the light on the sample which stretches the light spot in the horizontal direction by a factor of 3.6.

Plane VLS grating (nanospectroscopy)

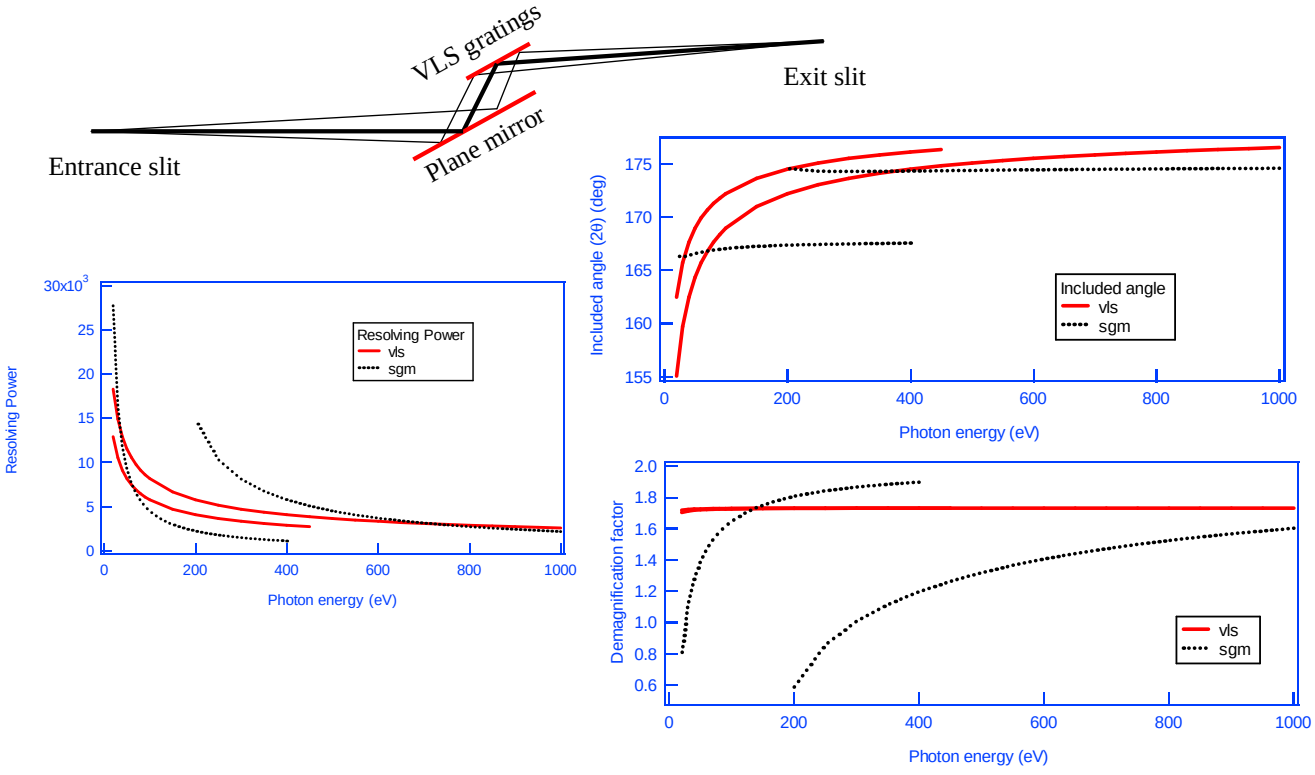

Microfocusing

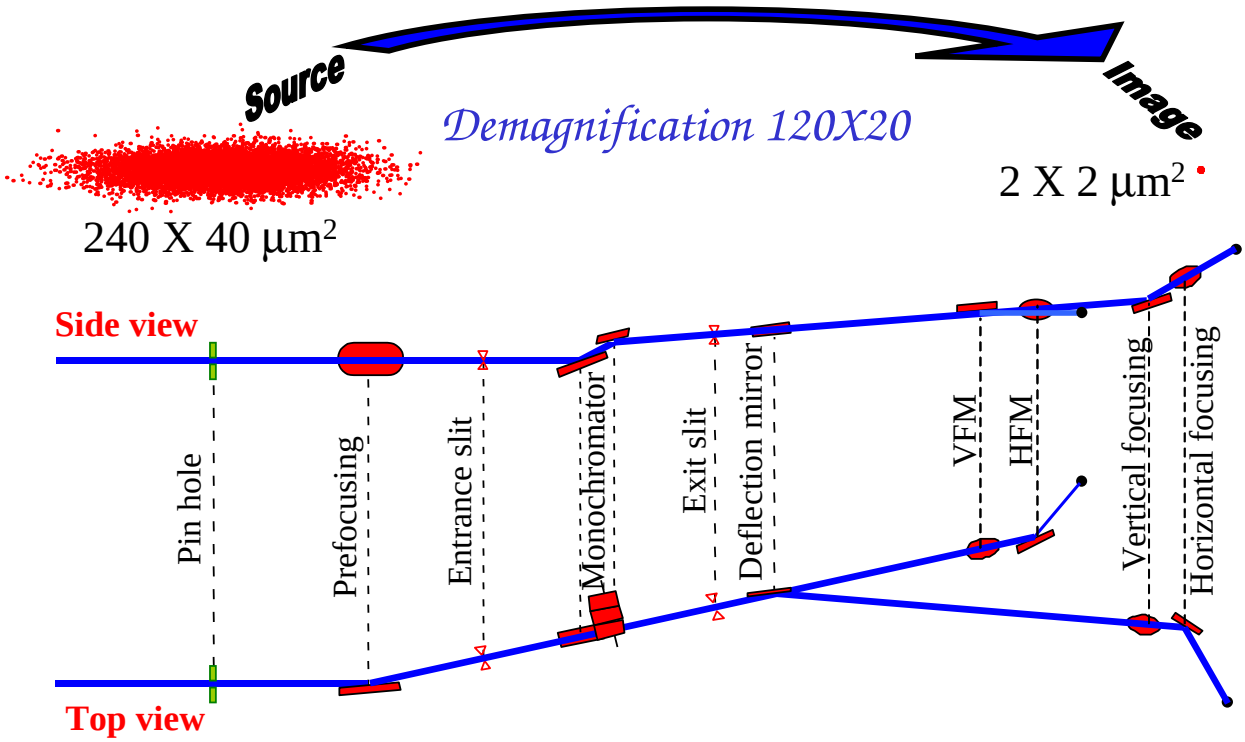

Microfocusing

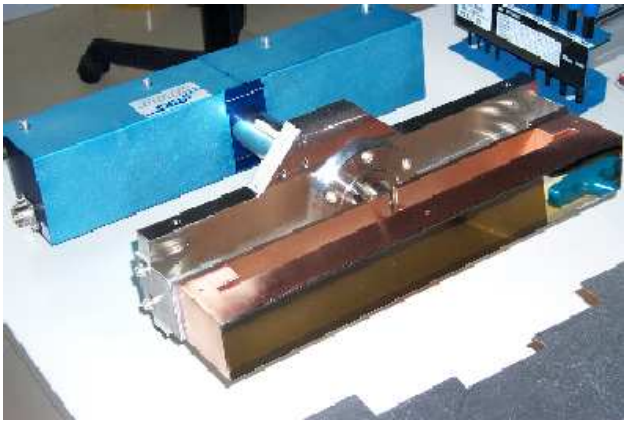

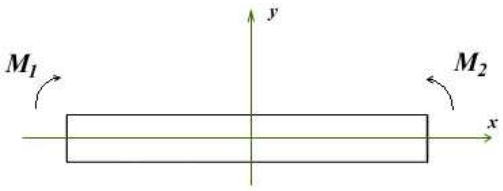

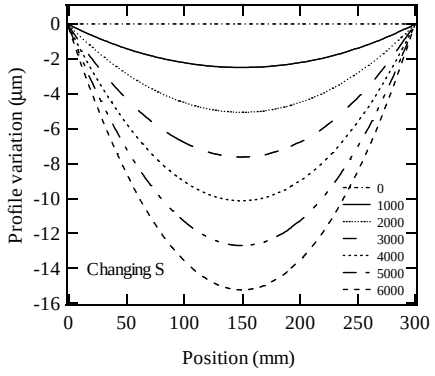

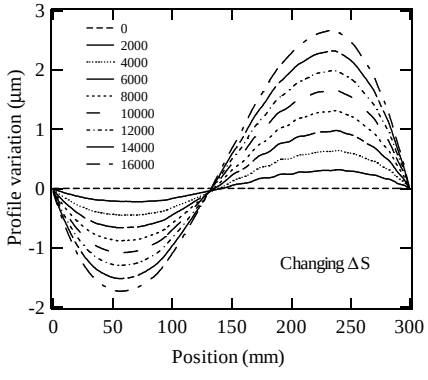

Microfocusing

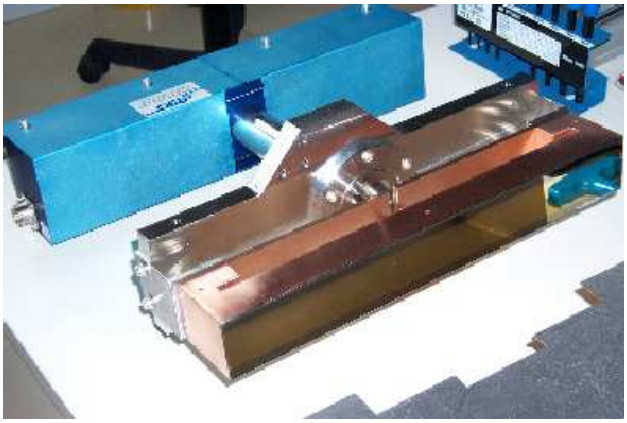

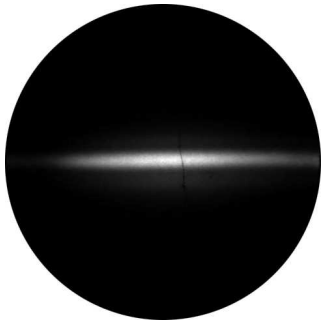

Sample tilted by 76°

2X7 μm^2

Flux $1x10^{13}$ ph/sec

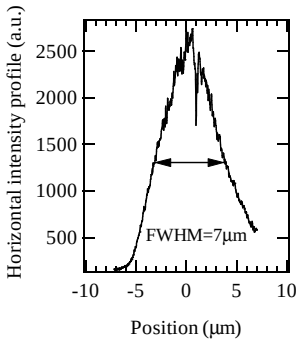

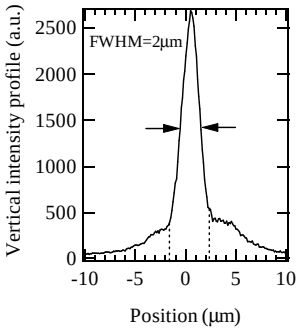

Focused photon spot on the sample in the SPELEEM microscope. The profiles are already corrected for the 16° grazing incidence angle of the light on the sample which stretches the light spot in the horizontal direction by a factor of 3.6.

Mechanical bender (ESRF)

micro-fluorescence & micro-diffraction (HXR)

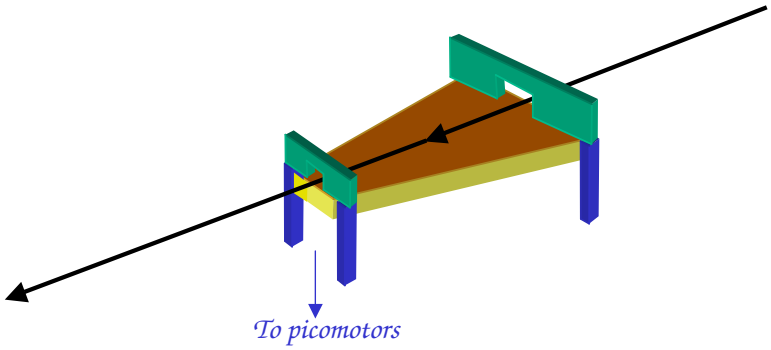

Bending system

The mirror must be shaped according to the required working distance and angle of incidence constant thickness but linear width variation.

Open clamping system to let the beam pass trough

Picomotors for the bending driving system (2 for each mirror)
Two different moments are applied at the end of the flat polished substrate

Active gratings

Surface equation $\xi = \sum_{i=0}^{\infty} \sum_{j=0}^{\infty} a_{ij} w^i l^j$

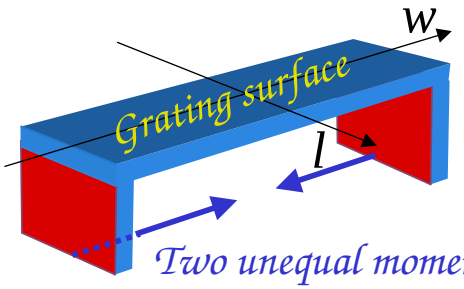

Two unequal moment applied

Via piezo motors.

3rd order shape correction

$$F_{20} = \frac{\cos^2 \alpha}{r} + \frac{\cos^2 \beta}{r'} - 2a_{20}(\cos\alpha + \cos\beta)$$ Grating focal equation

$$F_{30} = \left[\frac{T(r,\alpha)}{r}\right]\sin\alpha + \left[\frac{T(r',\beta)}{r'}\right]\sin\beta - 2a_{30}(\cos\alpha + \cos\beta)$$

3rd order aberration

Piezoelectric Bimorph mirrors

R. Signorato (ACCEL)
J.J. Fermé S.E.S.O.

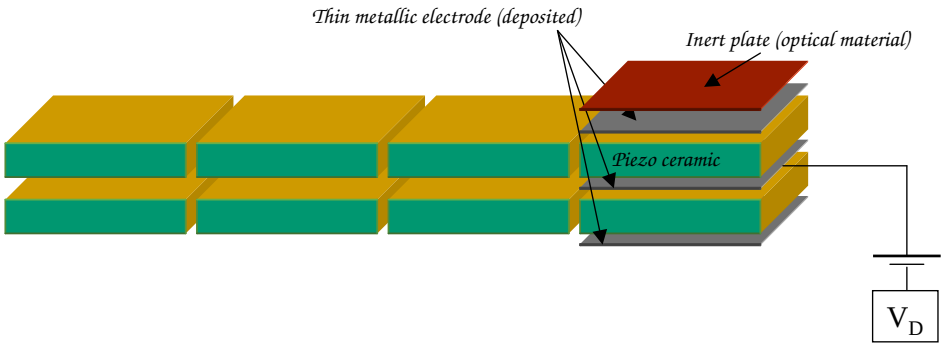

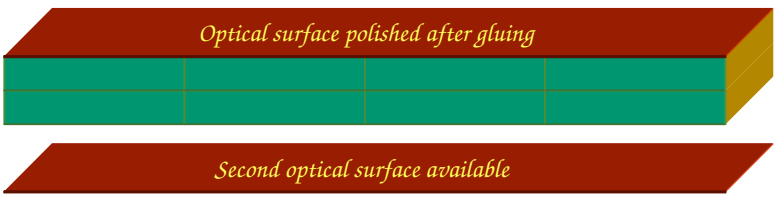

Piezoelectric Bimorph mirrors

Dimension: from 150 mm (single element) to 1400 mm.

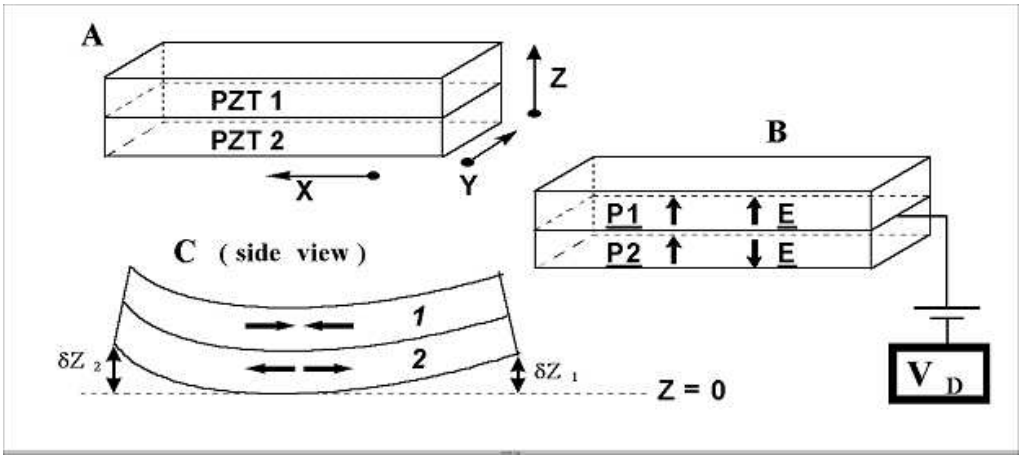

Radius variation: 370 m (+1500V) to 2300 m (-1500V)

Stability: $\Delta R/R \cong 0.8\%$ on 1 day scale
$\Delta R/R \cong 2.0\%$ on 10 day scale

Metrology

Since all the imperfection on mirrors and gratings will drastically reduced the performance a beamline precise characterisation of them is therefore mandatory.

In order to verify the compliance of the delivered mirrors and gratings before their acceptance and subsequent installation at a SR source beamlines, an optics metrology laboratory should be set up.

These are some instruments adopted in most of the SR laboratory around the world.

Fizeau-type interferometer (Zygo or Wyko). It is able to test flats up to 4 or 6 inches in length (direct view configuration), while in grazing incidence (autocollimation mode with a precision plane mirror) it is possible to test flats up to 500 (or more) mm in length. The accuracy for such instrument is of the order of $\lambda/20$, while the measurement repeatability is close to $\lambda/1000$ (λ=633 nm). To measure spherical surface or sagital radius is necessary to buy a reference sphere (typically quite expensive) or a transmission sphere.

Micro interferometer: (MICROMAP, WYKO etc..). It is able to provide 3D surface roughness measurements, with a repeatability better than 1 Å RMS, and a lateral resolution close to 0.5 µm. It is mainly used for mirror surface finish characterisation. Moreover, it is also helpful in order to check the groove density of gratings up to 600 lines/mm, or to characterise steps or defects on the optical surface. Sometimes it is also used to determine, in first approximation, the sagittal radius of curvature for cylinders or toroids, usually specified to be in the 30 mm to 100 mm range.

Non contact profilometer (LTP) Probably the most important instrument for grazing incidence optics. This instrument (Long Trace Profiler (LTP)) was developed at the Brookhaven National Laboratories by Takacs et al., and marketed by Continental Optical Corporation (actually Ocean Optics). It is basically a double pencil, slope measuring interferometer, able to measure the slope error and radius of curvature for optical surfaces up to 1 (or 2 depending on the configuration) m in length. Appropriately operated, it allows precise data acquisition, with a repeatability in the order of 5 nm P-V (or 0.1 µRad RMS). The LTP measurement principle is rather simple: while two pencil beams are scanning along the surface of a mirror, the reflected beam direction will change according to the local surface slope at that position. A Fourier transform lens, converts the angle variation of the reflected beam in a position's variation in its focal plane. The focused laser beam position is recorded by a linear array detector and, after a proper fit, the local slope of the mirror under test is obtained. The scheme of the instrument is the following:

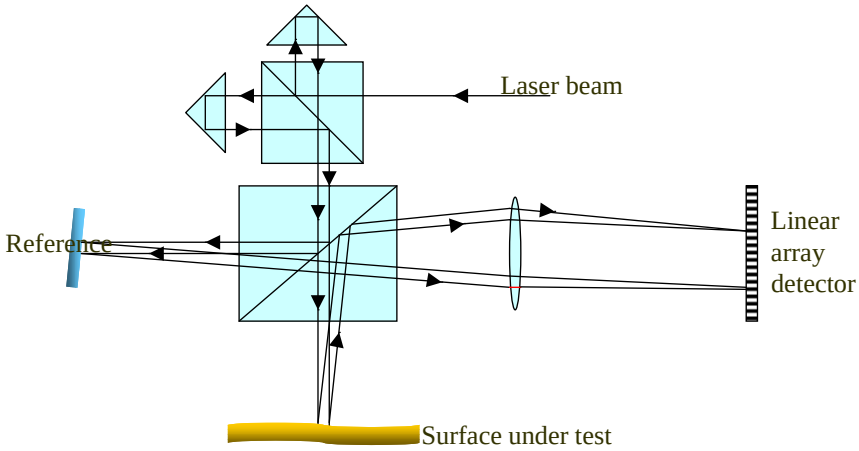

As with many other commercial instruments, sometimes it is necessary to “personalise” the as-supplied set up, in order to improve the capabilities of the instrumentation to match your requirements. Some major hardware improvements were undertaken at our metrology laboratory, to effectively increase the final accuracy of LTP. It was found that measurement noise was strongly reduced by substituting the original solid-state laser source with a He-Ne laser tube, connected to the optics head by means of a polarisation preserving optic fibre. Following an idea developed by S.N.Qian, a new set up for the LTP were developed: the penta-prism LTP, with stationary optics head and scanning penta-prism.

The main advantages of such a configuration were the introduction of an angle-maintaining penta-prism (less sensitive to the vibrations and the tilting errors of the scanning translation stage), a significant weight reduction of the movable part of the interferometer (with an obvious decrease of mechanical flexure of the scanning slide), and a side-mounting configuration for the surface under test (that greatly reduces the gravity induced deformation on the optical element under test).

After these significant hardware improvements, the other parameters to be optimised were related to environmental changes while measuring (mainly temperature stability and air turbulence along the laser beam path). In our experience, the temperature changes that occur on the brief to medium time scales (i.e. comparable to the time required to collect a set of data) have a direct influence on the He-Ne laser source stability (due to slight changes in the laser cavity tube), in the polarisation-preserving optics fiber that feeds the laser head, in the LTP optics head mechanical assembly, and in the thermal expansion of the scanned surface blank.

For this reason, in early 1995 we commissioned the construction of a temperature controlled room to host our LTP. This facility was ready at the end of that year, and has regularly operated since then. It consist of a double walled room, with adaptive temperature control by means of a circulating fluid system surrounding the hutch hosting the interferometer. Air circulation in the environment between the two walls ensures no thermal gradients from point to point of the inner hutch. Precise thermal monitoring at different points inside this inner room, has shown that the temperature stability achieved inside the room is of the order of +/- 0.2 ˚C, on time scale of several days. The same shielded environment, greatly reduces air turbulence in the laser optics path, enhancing the overall measurement accuracy.

With the same instrument it is possible to measure the groove density of the grating with a very high accuracy. Since the LTP is able to detect small angle deviations of the reflected laser beam due to a slope variation of the mirror under test, it is equally able to detect angle deviation of a laser beam diffracted (instead of reflected) by a grating. Nevertheless, to properly work with an LTP, the direction of the beam impinging the optics under test and the reflected one must coincide. For this reason,we should superimpose the incoming and diffracted beams. This condition is similar to the so-called Littrow condition where, the incoming beam and the diffracted one both coincide with the normal to the grooves. This is a condition that maximises the efficiency of a blaze grating but, in our case, it is absolutely not necessary that the beams directions coincide with the grooves normal. All we need is a beam diffracted in the direction of the incoming beam and therefore, the following equation should be satisfied:

$$\beta = \alpha \quad \rightarrow \quad 2d \sin\alpha = n\lambda \quad \rightarrow \quad 2\sin\alpha = nK\lambda$$

If the grating equation in pseude Littrow mounting could be satisfied (with λ=632.6 nm, i.e. the He-Ne laser source) one is able to measure the grating's grooves. Practically, one must rotate the grating of a well defined angle α_0 and after that make a scan with the LTP as if it was a mirror. The scan is made leaving the Optics head of the LTP fixed and moving only the penta-prism. Once a scan is obtained, we must consider that the measured angle deviation of the beam is a combination of two effects. One is the usual deviation of the diffracted beam due to the slope variation of the grating surface and the other is the deviation due to a change in the local groove density. As a matter of fact, it is evident that the measurement of the diffracted beam angle variation (δα) corresponds to the measurement of the local groove density, i.e.:

$$\sin\beta = \sin(-\alpha_0 + \delta\alpha) = \sin\alpha_0 - nK\lambda$$

Therefore, the desired parameter K, the groove density, can be directed obtained simply by making the sinus of the measured diffracted angle β. In reality, to be more precise, one should subtract the contribution due to the angle variation introduced by the slope of the surface. Hopefully this is not a problem because the local slope can be measured directly in the zero order condition, i.e. without rotating the grating, and therefore assuming the grating to be a common reflective surface, like a mirror. With this method, it is possible to measure groove density with a precision of δd/d< 10-6 equivalent to the measurement of the groove spacing with a precision better then 0.1 nm rms.

Metrology

Request of higher performance

SuperESCA 1991
Spot 20x200 μm2
Resolution 10000

Bach/Nanospectroscopy/APE 1998
Spot 2x2 μm2
Resolution 40000

Request of better mirrors

ellipsoids1″
Plane mirror 0.25″
gratings 0.2″

plane/sphere 0.1″
plane-elliptical mirror 0.1/0.2″
gratings 0.1″
Mirrors mounted on benders.

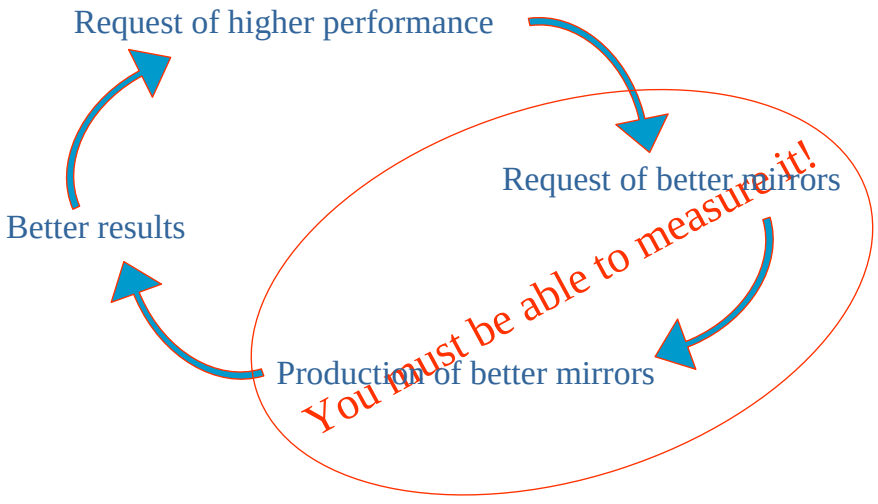

Metrology laboratory

Clean room class 1000 (BIOAIR)

Micromap Promap 512

Reichert POLIVAR 2 MET

Purchased in 1992
Roughness measurement
Good repeatability and precision (better then 1Å rms)

WYKO RTI 4100

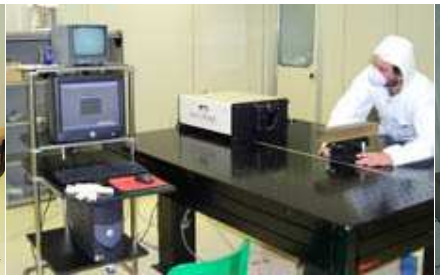

Purchased in 2002
3D surface topography

Thermostabilised room ($\Delta T = 0.1^{o}$ rms)

Long trace profiler (LTP II)

Purchased in 1991
Several in house modification
2D direct slope measurement

Long trace profiler (LTP)

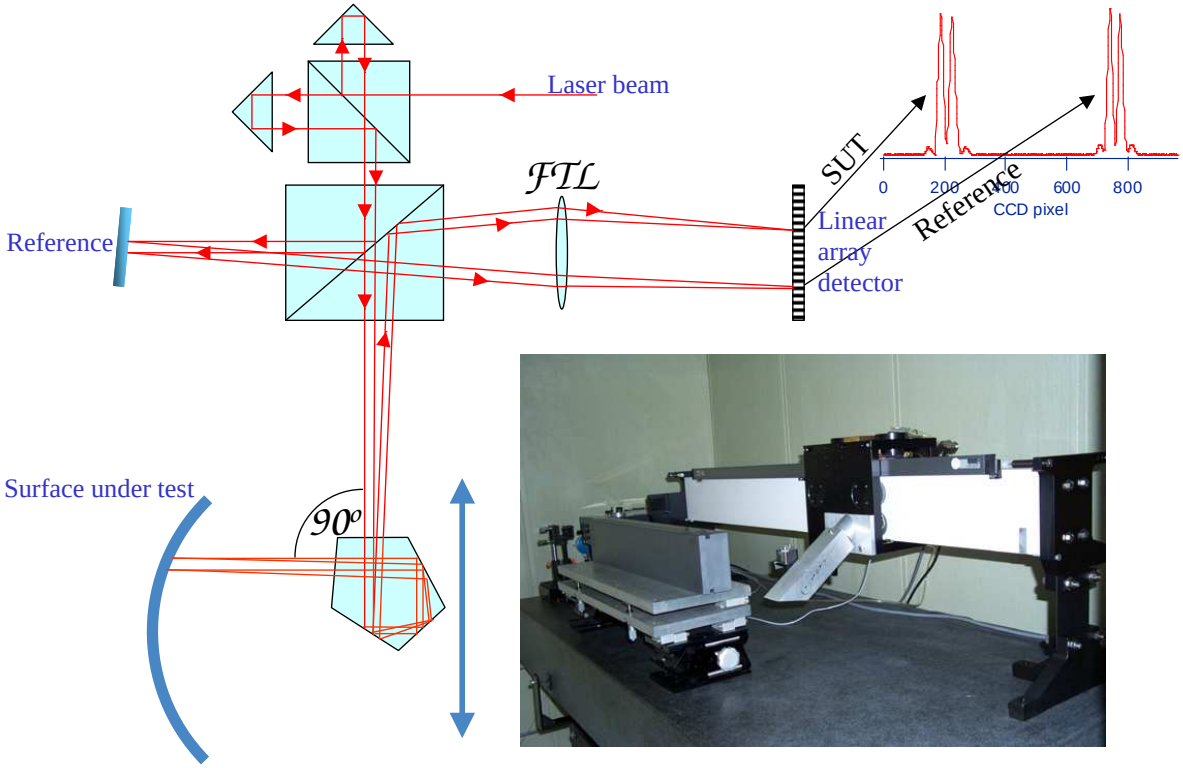

Long trace profiler (LTP)

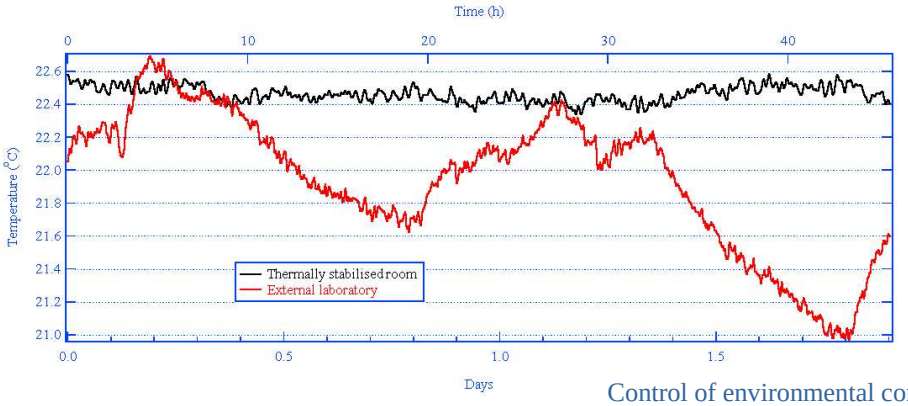

Control of environmental conditions
-Thermalisation of the laboratory
-Absence of air turbulence
-Remote control measurement
-Stable supports

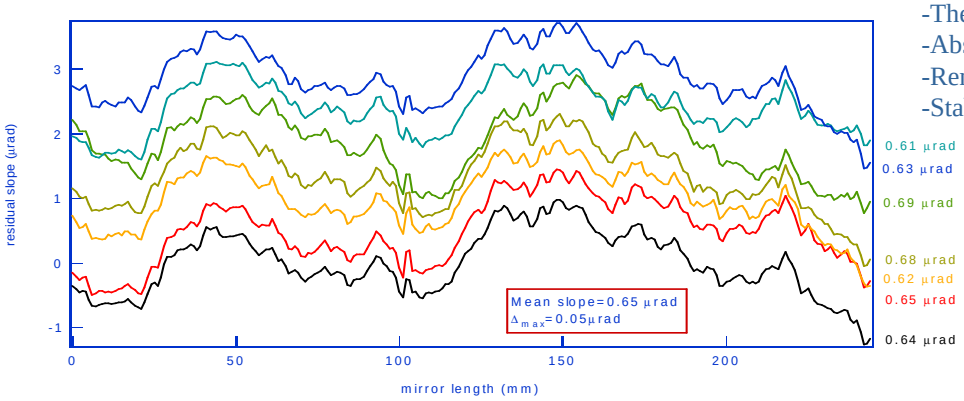

Groove density measurement

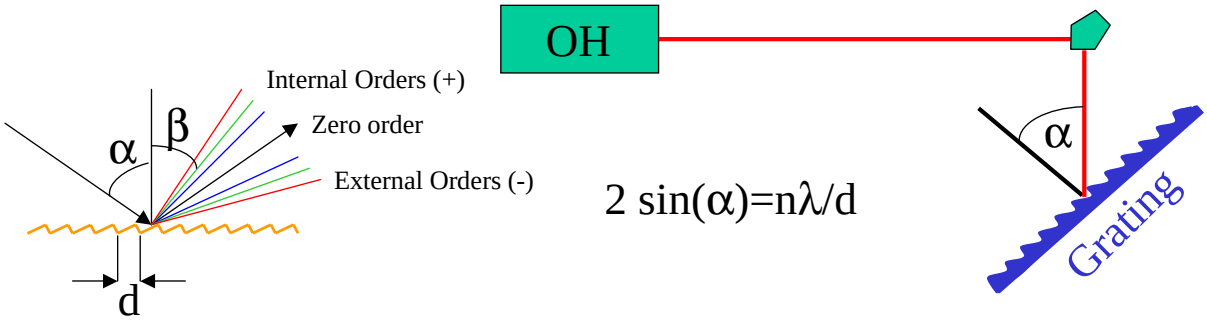

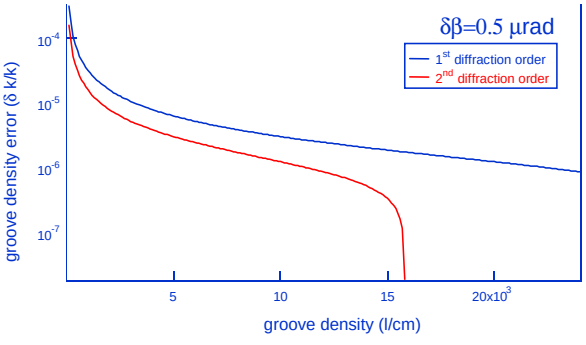

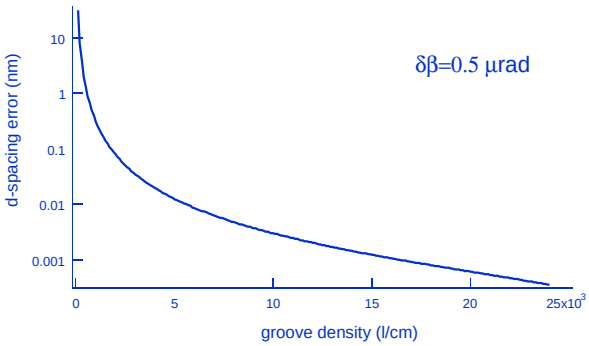

WYKO RTI 4100

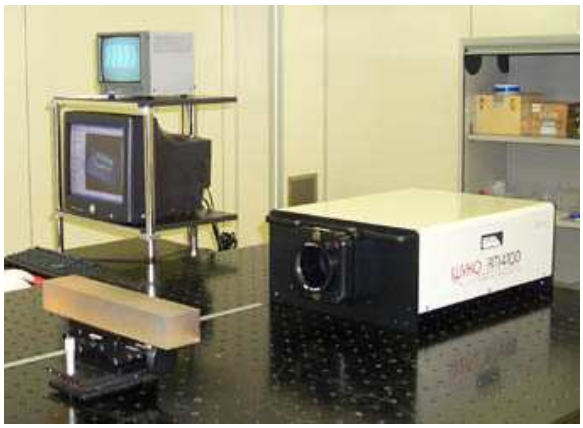

3D measurement of optical surfaces

λ/100 precision
λ/2000 repeatability

Accessories
Transmission spheres
f /1.5 for sagittal radii and NI mirrors with R<1 m
f /24.8 diverger for NI mirrors with R>2 m

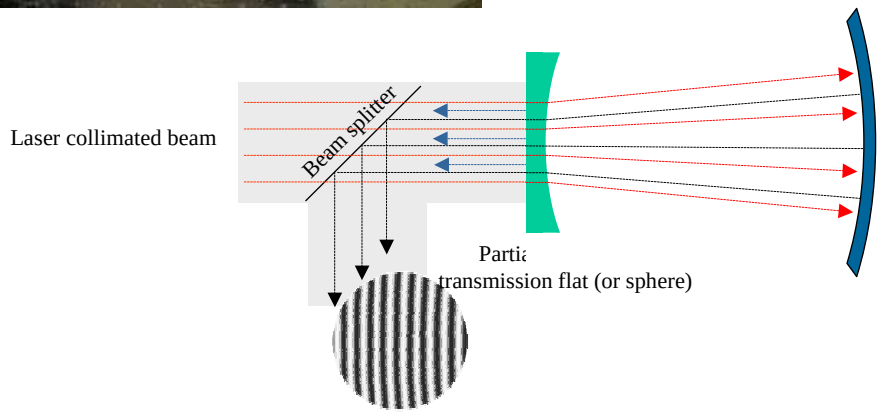

Bibliography

Books:

W. B. Peatman: *Gratings Mirrors and Slit* Gordon Sci. Publ. Amsterdam (1997)

D L Ederer *Selected Papers on VUV Synchrotron Radiation Instrumentation: Beam Line and Instrument Development* SPIE vol. MS152 (1998)

P. Z. Takacs, T. Tonnessen *Materials, Manufacturing and measurement for Synchrotron Radiation Mirrors* Spie Proc. 3152 (1997)

W.R. McKinney, C.A. Plamer *Theory and Practice of Surface-Relief Diffraction Gratings: Synchrotron and other applications* Spie Proc. 3450 (1998)

CXRO *X-ray data booklet* Lawrence Berkeley Nat. lab. (2001) free

Programs:

Shadow (ray tracing) http://www.nanotech.wisc.edu/shadow/shadow.html
XOP (general optical calculation) http://www.esrf.fr/computing/scientific/xop
SPECTRA (synchrotron source) http://radiant.harima.riken.go.jp/spectra/index_e.html

Links:

Centre for X-ray Optics http://www-cxro.lbl.gov/ *(general information and on line software)*
The international society for Optical Engineering http://www.spie.org
Optics.org http://optics.org
Photonics.com http://www.photonics.com/
Soft X-ray group of Elettra: http://www.elettra.trieste.it/organisation/experiments/laboratories/soft_xray